INORGANIC CHEMISTRY
FRONTIERS

REVIEW

View Article Online
View Journal | View Issue



Cite this: *Inorg. Chem. Front.*, 2022, **9**, 3943

# Post-synthetic modification of Prussian blue type nanoparticles: tailoring the chemical and physical properties

Ekaterina Mamontova, [a] Fabrice Salles, [a] Yannick Guari, [a] Joulia Larionova [a] and Jérôme Long *[a,b]

Received 17th May 2022,
Accepted 4th July 2022

DOI: 10.1039/d2qi01068b

rsc.li/frontiers-inorganic

Prussian blue (PB) type nanoparticles belong to an exciting family of molecule-based nanomaterials. They combine the possibility of surface engineering with specific advantages related to their porous molecule-based structures and their fascinating chemical and physical properties including redox, magnetic, photothermal and host–guest features. In this review, we focus on recent advances in the Post-Synthetic Modification (PSM) of nano-sized PB and its analogues (PBA) and compare them with the current strategies used in Metal–Organic Frameworks (MOF) in order to give the outlooks on the future researches in this domain.

## 1 Introduction

Since their discovery more than three centuries ago, Prussian blue (PB) and its analogues (PBA) have fascinated various scientific communities.[1] These molecule-based systems are undoubtedly recognized as the first coordination network-based materials, in which transition metal ions are assembled through bridging cyano ligands to generate a three dimensional cubic structure of general formula $A_{1-x}M[M'(CN)_6]_c\square_d$ (A is an alkaline ion, M and M′ are transition metal ions and □ denotes the hexacyanoferrate vacancies).

More specifically, their synthesis at the nanoscale, for which the starting point could be traced back about two decades ago,[2,3] has opened tremendous opportunities for the development of new functional materials having applications in multiple fields ranging from batteries to biology and

[a]*ICGM, Univ. Montpellier, CNRS, ENSCM, Montpellier, France. E-mail: jerome.long@umontpellier.fr*
[b]*Institut Universitaire de France (IUF), 1 rue Descartes, 75231 Paris Cedex 05, France*

**Ekaterina Mamontova**

*Ekaterina Mamontova obtained her PhD degree (2020) in material chemistry from the University of Montpellier. Her scientific interests concerned the development of new functional (nano)materials for different applications: catalysis, sensors, biomedicine. From 2020 to 2021, she was in charge of organizational, administrative, and communication management of a European research project coordinated by CNRS-LHFA (Toulouse). Currently, she is Research Project Manager at the Innovation and Partnerships Department of the University of Montpellier.*

**Fabrice Salles**

*Fabrice Salles, 42 years old, received his PhD from UPMC (Paris, France) in 2006. After Post-Doctoral Fellowships at the Royal Institution of Great Britain in London (UK), in the group of Prof. C. R. A. Catlow, and at the ICGM from Montpellier, he became CNRS researcher in 2010 and obtained his "Habilitation to Direct Research" in 2016 from the University of Montpellier. His research interests consist into the determination of crystal structure and combining classical and DFT simulations to design new nanoporous materials, elucidate adsorption and diffusion mechanisms, and predict their performances for energy, health and environment applications.*

medicine.[4,5] Such interest is related to the specific molecule-based nature of PB and PBA, which confers to these nanosystems different physical, chemical and mechanical properties compared to classical inorganic nanoparticles.[6–12] In a similar fashion that their so-called Metal–Organic Frameworks (MOF) congeners, PB and PBA exhibit remarkable advantages, such as optical transparency, low density and easy synthesis in soft conditions. Besides, one of their main assets lies in their important chemical and structural flexibilities which affords: (i) a versatility in terms of chemical compositions through the careful choice of the metal ions giving rise to various functional properties (magnetism, optics, conductivity); (ii) an internal porosity that may allow the encapsulation of various species; (iii) a high chemical and thermal robustness in various media (including water over a large neutral and acidic pH range) making them particularly adapted for numerous applications.[9,11]

Future innovations necessitate however to progressively and carefully adjust the properties of nanomaterials with applications encompassing biomedical area, sensors, microelectronics, catalysis, gas or water treatments, and others.[13–17] Moreover, owing to their myriad of different properties, PB and PBA nanoparticles could be classified as intrinsically multifunctional materials,[18] but the implementation of additional physico-chemical properties will greatly unleash the full potentiality of these original nanosystems.

In this context, the Post-Synthetic Modification (PSM), which consists in modifying the surface of nano-objects with functional groups or/and integration of some species within the porosity of previously synthesised systems, has widely been employed in the case of classical metal/metal oxides nanoparticles,[19,20] quantum dots,[21] silica nano-objects,[22,23] MOF[24,25] and others. This approach allows customizing nano-objects with new functional groups or entities without affecting their structural integrity in the aim to change the existing physical, chemical, pharmacological, mechanical properties or implement new ones. More importantly, PSM may give access to functionalized materials that could not be obtained by a direct synthetic route.[25,26] Besides, PSM also allows establishing direct comparison between unmodified and modified nanosystems to monitor the improvement of the functionalization. The advantages of the PSM consist in the possibility: (i) to introduce functional groups incompatible with the conditions of the initial synthesis, (ii) to introduce new functional groups or species with desired properties, (iii) to easily design multifunctional materials.

With this in mind, PB and PBA nanoscaled systems benefit from two important features found also in MOF: their surface may be functionalized, and their porosity may be filled with guest molecules or cations of appropriated size. The PSM could be performed at different levels. The surface functionalization of PB and PBA by various ligands, organic dyes, polymers and biopolymers, antibodies ensures the modification of their physical, chemical and pharmacological properties bringing indeed additional luminescence, improved blood circulation, biocompatibility and the stealth character of nanoparticles for their use as nanoprobes or therapeutic agents. Moreover, the modification of nanoparticles' intrinsic porosity can also give them additional functionalities (possibility of drug delivery, optical properties for fluorescent dyes and complexes). Although the term "PSM" has been widely employed in the field of MOF in their bulk form for more than 15 years, it has never been formalized and designated in the case of PB/PBA nanoparticles, although examples of surface modifications have appeared just a few years after the first report of the nanoscale synthesis of PB.

**Yannick Guari**

*Yannick Guari is head of the Molecular Chemistry & Materials Department at the Institut Charles Gerhardt Montpellier, University of Montpellier, France, and conducts research on metal-containing nanoparticles and nanocomposites. He earned a PhD in chemistry at the University of Toulouse in 1998. His thesis work under the supervision of Bruno Chaudret was on ruthenium complexes and their uses for the C–H bond activation. After a postdoctoral stay at the University of Amsterdam in the research group of Prof. Piet van Leeuwen, studying palladium and platinum complexes in homogeneous catalysis, Dr Guari joined the CNRS, France, as a permanent researcher in Montpellier where he conducts research on inorganic nanoparticles.*

**Joulia Larionova**

*Joulia Larionova is an engineer in radiochemistry. After defending her thesis at the University of Bordeaux in 1998, she completed a post-doctoral fellowship in Switzerland and was appointed as a Lecturer at the University of Montpellier. Being a full Professor at the University of Montpellier since 2009, she directed research activities in the Institute Charles Gerhardt Montpellier (ICGM). Her research topic is focused on the development of inorganic and molecular materials at nano- and macro scale with magnetic and optical properties for applications in the areas of electronics, biology and medicine.*

Most of inorganic nanomaterials (metal, metal oxides, quantum dots) are not porous and could only be functionalized through their surface modification. The approaches for this latter have been known for decades and numerous books and reviews have already been dedicated to this topic.[19,20,27–30] PSM of silica nanoparticles can be achieved through both, modification of their porosity and surface, which have been very well documented in the literature.[22,23,31–33] On the other hand, the use of the PSM strategies applied to molecule-based nanomaterials, such as MOF, has only been recently reviewed since the history of these nanoparticles started only around twenty years ago.[34–36] Whereas PSM is widely employed in the literature, its systematization for nanoscaled PB and PBA has been only scarcely addressed up to now.

In this contribution, we will provide an overlook on the PSM approach in nanoscaled PB and PBA. Given the similarities between MOF and PB/PBA, we will firstly give a brief overview concerning the general strategies of PSM of the internal porosity of bulk MOF, which can be transposed to PB/PBA. Second, we will discuss the synthesis of PB type nanoparticles. Third, the description of different methodologies used in the literature to post-functionalize PB/PBA either by modification of the internal porosity or using surface engineering will be then carried out. In the last part, we will shed light on the benefits of such approach in terms of different applications and draw some perspectives.

## 2 Post-synthetic modification in MOF

Functionalisation of the pores and/or the external surfaces have been investigated in MOF to implement specific host–guest interactions or introduce particular metal ions. While modification of solvents or encapsulation of drugs can also be considered as PSM, we will focus in this part on the chemical modification of the frameworks (such as a metal ion exchange, substitution or introduction of ligands, *etc.*) on the external surfaces,[37,38] or functionalization of the internal porosity.[25,39]

### 2.1 Pores or framework functionalization in MOF

Most of the works devoted to PSM in bulk MOF have focused on functionalizing the internal porosity of their structures. The reader can refer to detailed reviews for further details.[24–26,40,41] Briefly, this strategy allows the systematic modification of the MOF structure through chemical reaction in its internal porosity and in turn gives access to functional MOF, which could not be obtained from a direct synthesis due to incompatible synthetic conditions or high reactivity. The reaction proceeds through diffusion of the reactants into the pores of the framework to interact either with the ligands or metal centres. The structural integrity of the framework is preserved and the reaction is generally performed in a solid/solution system, although solid/gas and solid/solid PSM reactions could also be carried out.[42,43] Different PSM routes have been categorized (covalent PSM on the linker, coordination/covalent modification of the metal ion and combination of both approaches, PSM metal exchange, PSM ligand exchange, PSM deprotection, *etc.*).[24–26]

Historically, the first PSM in MOF deals with modification of the organic linkers and has been reported by Wang *et al.* in 2007 by performing a simple organic chemistry reaction (amide formation) in the IR-MOF3 (IR = isoreticular) using the free amine available on the linker.[44] Remarkably, such reaction takes place in the porosity of the framework, highlighting the high chemical robustness of the MOF system to allow the chemical modifications without degrading the structural features. The same year, Dincă *et al.* have proposed the metal ions exchange in a manganese-based MOF,[45] while Kim and co-workers have modified an achiral MOF into an active chiral catalyst by coordination of a chiral L-proline derivative on the unsaturated metal centers.[46] Small molecules could be adsorbed within the MOF porosity and react with either the ligands or the metal ions,[47–49] or, in other terms, with basic and acid Lewis sites.[41]

The presence of functional groups on organic linkers, or the availability of active metal centres, which could interact with various species *via* covalent or coordination bonds, open the way to multiple reactions for a considered MOF. Besides, the possibilities are almost infinite since sequential steps PSM could be carried out to finely tune the features of MOF. More than thousand articles have been published demonstrating indeed the success of this approach in the field of MOF. However, some challenges still remain, such as the influence of different factors on the modifications (*e.g.* ionic radii, coordination geometry, crystallite size, $pK_a$ of the linker, *etc.*).[25]

Naturally, one obvious synthetic strategy to post-functionalize MOF consists in loading functional guests inside their pores, and sometimes referred as a "ship-in-a-bottle" strategy.[50] Since the pore size and chemical functionalities may be adjusted in MOF, the nature of the guests could be miscellaneous and ranges from organic molecules, dyes, drugs, metal

**Jérôme Long**

*Jérôme Long has been Associate Professor at the Institut Charles Gerhardt, University of Montpellier since 2010. He received his PhD from the University Pierre and Marie Curie (Paris VI) in 2009 under the supervision of Dr V. Marvaud. He undertook a post-doctoral stay at the University of Ottawa with Prof. M. Murugesu. He was appointed in 2021 at the Institut Universitaire de France (IUF). His current research is oriented towards the design and characterization of multifunctional molecular materials including lanthanide-based systems and porous coordination frameworks.*

complexes, cluster or nanoparticles with applications in gas adsorption, catalysis, drug delivery or sensors.[49,51–56]

More generally, the PSM permits to modify the properties of MOF, such as the hydrophobic/hydrophilic balance, the pore size, the framework stability, the catalytic features as well as magnetic and conductivity properties.

Yet, the PSM requires that: (i) the windows pore size of the MOF should be compatible with the size of the molecular precursor or guest that needs to diffuse into the porosity of the framework; (ii) the reaction conditions should be compatible with the chemical/thermal stability of the MOF. For instance, some MOF often exhibit water instability, which prevents them from being considered for several applications, such as gas separation in a humid atmosphere.[57] For this reason, different strategies have recently been developed to circumvent this weakness.[58,59] In addition, various approaches have been followed to tune the hydrophobic–hydrophilic balance in MOFs. Indeed, it is possible to modify the hydrophobic character by changing the nature of the ligand and/or the metal centre by PSM.[60] Inclusion or incorporation of different materials inside the pores can also modify the behaviour of solids and in particular their affinity for water. It has thus been possible to change the hydrophobic Cu-BTC (BTC = benzenetricarboxylate) framework into an hydrophilic solid by incorporating hydroxide double lamellar sheets inside the porosity.[60] Similarly, the introduction of amino-acids in UPG-1(Zr) (UPG = University of Perugia) has increased the hydrophilicity due to a greater confinement effect.[61] Finally the hydrophilicity of MOFs (MIL-101 (Cr), MIL = Materials Institute Lavoisier) has been enhanced by introducing alkali cations, which allows a tunability of the hydrophilic character.[62] More generally, the introduction of cations inside the porosity, can not only modify the hydrophobic–hydrophilic balance but can also have an impact on the diffusion of guest molecules and therefore enhance the interactions between drugs and framework.[63]

### 2.2 Surface functionalization in MOF

All the previous examples concern the successful modification of the internal porosity, but selective surface engineering or functionalization of both, surface and internal porosity have also been reported in the literature.[64,65] Modifying the external surface of MOF has however received far less attention with respect to the internal porosity functionalization despite the potentialities to adjust physical and chemical properties, such as stability and dispersibility, or enhance a selective guest uptake.[52,66–68] Using comparable methodologies that those found for inorganic nanoparticles, various chemical interactions could be involved to perform post-synthetic surface modifications of MOF.[34–36] This often relies on the use of large reactants or surface ligands that could not enter into the porosity of the coordination framework, and which in turn provide specific surface properties (*e.g.*, solubility, *etc.*). For instance, polymers, such as poly(vinylpyrrolidone) (PVP), alkyl-modified chitosan, dextran or polyethylene glycol (PEG), could be attached on the surface of different MOF ([Ln(1,4-bdc)$_{1.5}$(H$_2$O)$_2$],[69] MIL-88A and MIL-100[70]) due to their large size that prevents their diffusion into the pores. Other examples include coating of MOF with lipids[71] or a porous polymer.[72] The nature of the interaction between the surface agent and the MOF may vary depending on the presence of coordinative functions on the latter.

In this sense, using ligands able to provide strong chemical interactions with the MOF surface (such as coordination or covalent bonds) offer further alternatives. Hence, the post-synthetic exchange of ligands could be performed. Such approach has been firstly demonstrated on a zinc coordination network incorporating carboxylate ligands[73] that could be exchanged on specific single-crystal surfaces using a fluorescent boron dipyrro-methene (BODIPY) linker exhibiting a carboxylate group that could substitute the pristine linker. Due to the large steric hindrance of the BODIPY linkers, the exchange is only restrained at the surface, as evidenced by atomic force microscopy (AFM). Such methodology was later applied to others MOF, such as HKUST-1 (HKUST = Hong-Kong University of Science and Technology) or ZIF-8 (ZIF = Zeolitic Imiadazolate Framework).[74,75] RAFT co-polymers containing a thiolate function could also be attached through a coordinative bond with the $Gd^{3+}$ ions on the particles' surface.[76] Remarkably, the used copolymer incorporated a fluorescent tag, a targeting ligand and a therapeutic agent, resulting in a MOF that could be used as a theranostic nanodevice.

The exchange of species at the surface is not only limited to ligands but can also involve metal ions through transmetallation reactions. However, this appears much difficult to control due to the diffusion of the metal ions within the porosity of the framework.[52,67,68] Yet, multistep surface functionalization could also be achieved to specifically tune the surface, including the nature of the metal ions. For example, the thermal activation of MIL-101(Cr) creates coordinatively unsaturated sites that are able to react with dopamine.[77] The catechol functions of this latter were protected with bulky groups to limit the reactions exclusively on the surface. Upon attachment at the surface through the amine functions, the deprotection provides a bidentate binding site that is able to subsequently react with the transition metal complex [VO(acac)$_2$] (acac = acecylacetonate) yielding to a catalytically active functionalized system. Functionalisation of the surface can also protect the solid from the aggression of the external environment, such as pH effect, by modifying the charge distribution due to reduction of surface active elements.[78]

Recently, various biomolecules (amino-acids,[79] peptides,[80] oligonucleotides[81,82]) have been used to functionalize the surface of MOF nanoparticles for biomedical applications. The possibility to perform bioconjugation using the carboxylate linkers through classical EDC (1-ethyl-3-(3-dimethylaminopropyl)carbodiimide) or DCC (*N*,*N*′-dicyclohexylcarbodiimide) couplings or even proteins constitutes also a facile route.[83] In a similar vein, the use of surface "click chemistry" using for instance azide/alkyne reaction for targeted applications has also emerged in the last few years.[84] Modifications of external surfaces in nanoscaled-MIL-100(Fe) with biopolymers has thus proved to be efficient to enhance

 

the interactions with active drug molecules[85] or to allow the cutaneous administration of cosmetic molecules.[86,87]

# 3 Design of Prussian blue type nanoparticles

## 3.1 General considerations about bulk PB and PBA

PB is the first coordination network discovered around 1706 in Germany.[4,88] The wide range of PB/PBA properties embracing electronic, magnetic, optical or host–guest properties has given rise to various applications in catalysis,[89] energy storage,[90–93] waste decontamination,[94] gas storage,[95–97] biology and medicine.[4,5,10,98] PB is a mixed-valence system with the chemical formula $Fe^{III}[Fe^{II}(CN)_6]_{3/4}\square_{1/4}\cdot nH_2O$. Remarkably, the $Fe^{II}$ and $Fe^{III}$ ions could easily be substituted by other transition metal ions to obtain a variety of PBA compounds of general formula $A_{1-x}M[M'(CN)_6]_c\square_d\cdot nH_2O$ without affecting the resulting structure, which allows to directly probe the influence of the metal ions over the resulting properties. The network could be described as a "simple" face centred cubic (*fcc*) structure, reminiscent of NaCl. Besides, PBA structures with lower symmetries (mainly monoclinic,[99,100] tetragonal[101,102] or rhombohedral[103,104]) have been reported depending on numerous parameters (nature of the metal ions, redox reactions between the metal centres, nature of the guests/ions and temperature). This appears particularly relevant for batteries applications since structural transitions could be observed during the ion charge/discharge process.[93,105]

In their bulk form, PB/PBA have been widely synthesized in aqueous solutions[95,106] by reaction between a hexacyanometallate complex, $[M'(CN)_6]^{p-}$, and a hydrated metal cation, $[M(H_2O)_6]^{n+}$. The ambidentate character of the $CN^-$ ligand allows to bind selectively two metal ions with an almost linear angle, which leads to a three-dimensional coordination network, made up of perfectly defined M′–CN–M sequences. However this simple structural description does not reflect the high complexity of the atomic-scale arrangement and for which the in-depth understanding still remains a challenge, as we will describe *vide infra*.[1,107]

Depending on the experimental conditions during the synthesis, alkaline cations (A) present in the reaction medium could be inserted into the tetrahedral sites of the *fcc* structure (Fig. 1A). This leads to a wide range of chemical compositions for a unique pair of transition metal ions, limited by two extreme formulas: lacunar $M[M'(CN)_6]_{2/3}\square_{1/3}$ ($Fe[Fe(CN)_6]_{3/4}\square_{1/4}$ for PB) and non-lacunar $AM[M'(CN)_6]$ forms (Fig. 1A and B).

Thus, the electroneutrality of the solid in lacunar structures is ensured by hexacyanometallate vacancies. As a direct consequence, water ligands complete the coordination spheres of $M^{n+}$ ions in the vicinity of these lacunas to satisfy their usual octahedral geometry. The average environment of these ions is estimated as four cyano ligands and two water molecules and could be formulated as $[M(NC)_4(H_2O)_2]$. We would like to emphasize that, however, this mean description does not reflect the distribution in coordination environments generated from the random arrangement of the vacancies in the network.[108] In addition, two other types of water molecules (lattice and zeolitic) may occupy the porosity of the framework. Water molecules of different nature may easily be identified by thermal gravimetric analysis since their loss could occur in a more or less stepwise manner.[109]

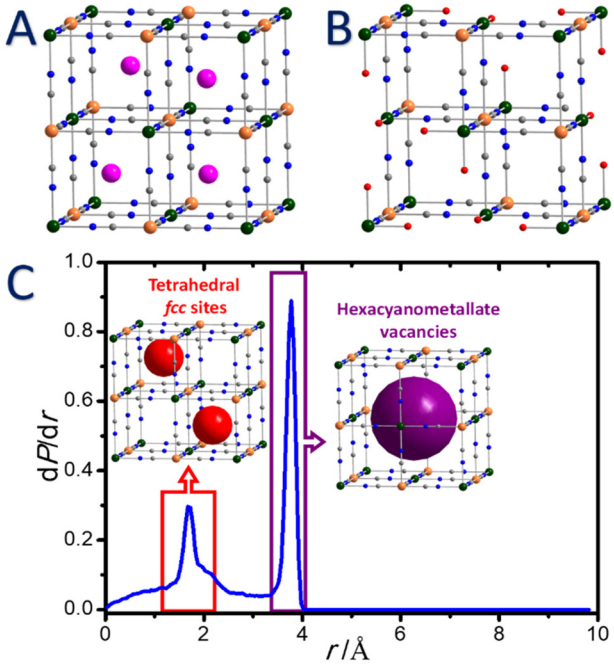


**Fig. 1** Crystalline structure of non-lacunar (A) and lacunar (B) PBA, $A_{1-x}M[M'(CN)_6]_{1-x/3}\cdot nH_2O$. Colour code: orange, M′; green, M; magenta, $A^I$; blue, N; grey, C. The oxygen of $H_2O$ coordinated to the $M^{n+}$ ions are represented by red spheres; (C) pore size distribution of PBA obtained from Monte Carlo simulations illustrating the presence of two types of pores corresponding to the tetrahedral sites of the *fcc* structure and the larger pores formed by hexacyanometallate vacancies.

In addition to the pores corresponding to the tetrahedral sites of the *fcc* structure, the presence of hexacyanometallate vacancies conducts to the creation of larger pores (Fig. 1B and C), which are particularly important to perform PSM. We would like to point out that the study of the concentration and ordering of the hexacyanometallate vacancies remains extraordinarily complex and directly affects some physico-chemical properties of PB and PBA. It is therefore more and more admitted that the vacancies arrangement is in some extent ordered in the solids and is also dependent on the chemical composition of the PBA.[1,107,108,110,111]

The presence of vacancies PBA is also strongly dependent on the experimental conditions during the synthesis. Understanding the atomic scale arrangement of vacancies within the coordination network implies elucidating the diffusion mechanism in these PBA.[112] Recently Simonov *et al.* have shown that the vacancies are not randomly distributed but are somehow ordered in the structure, which allows adjusting the targeted properties for molecules or ions diffusion and

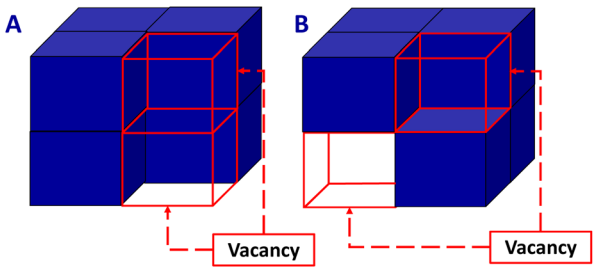


Fig. 2 Description of PB/PBA structure containing a vacancy pair (A) or vacancy-pair free (B). Adapted with permission from ref. 112. Copyright 2019 American Chemical Society.

authorizes the transport throughout the crystal structure.[107] In addition it appears that the vacancies are connected to create a percolation path and the presence of vacancies pairs can be observed (Fig. 2).[112]

First-principles calculations have investigated these arrangements and evidenced that the vacancy pair free configurations are the most favourable at 300 K.[112] Although, based on different molecular precursors, it has also been shown that the long distance order can be observed for vacancies of $[Bi(SCN)_6]^{3-}$ in the thiocyanate analogues of PBA.[113] It has further been proved that adjustment of the size of the vacancies might be achieved by introducing polynuclear cyano complexes with a octahedral arrangement instead of the usual mononuclear hexacyanometallates.[114]

In PB/PBA, the porosity allows to encapsulate or transport guest ions or molecules of appropriate size and shape (such as $H_2O$, $NH_3$, $CH_4$, $CO_2$, $H_2$, *etc.*).[95–97,106,115–121] However, their porous character drastically differ from their MOF counterpart at several levels: (i) in contrast to numerous MOF, the nature of both, the metal ions and hexacyanometallate moieties could be modulated without affecting the resulting framework topology. Indeed, in MOF solids, the chemical versatility can lead to a variety of porous structures with different dimensionalities (1D, 2D, 3D, presence of cages, *etc.*) and different pore sizes,[60–62] which impact the adsorption of small gases. In contrast, PB and PBA structures present an organized porosity due to the presence of channels and vacancies which are only slightly affected by chemical modifications.[112] This allows to decipher the influence of the metal ions over the adsorption features; (ii) the small cubic pores in PB and PBA also offer a high content of π density arising from the cyano groups that could be beneficial to capture certain molecules; (iii) the existence of structural flexibility in MOFs (such as MIL-53 (MIL = Matériaux de l'Institut Lavoisier) or Co(1,4-benzenedipyrazolate) for instance) can drastically modify the adsorption of gases and vapors,[122,123] while the mechanical stability of PB/PBA assures a constant adsorption saturation.

Moreover, the porous character of PB and related analogues in association with the presence of alkaline ions in the tetrahedral sites of the PB/PBA structures is attractive for the separation or insertion of small hydrated cations, such as $Na^+$, $K^+$, $Rb^+$, $Cs^+$, and $NH_4^+$, which is useful for different applications: membrane for ions separation,[124] component for batteries,[91,103,125] or for selective trapping of these cations in waste purification or radioactive ions decontamination.[126] Compared to conventional zeolites, the $Cs^+$ adsorption performances appear excellent due to the high affinity of the PB network for this cation. In particular, the mechanism of radioactive and non-radioactive caesium and thallium ions capture by PB has been investigated since the 1960s in the aim to enhance the excretion of these ions from the human body.[127–131] It has been evidenced from both, human and animal studies, that insoluble form of the bulk PB is an efficient antidote against $Cs^+$ and $Tl^+$ poisoning. In 2003, the U.S. Food and Drug Administration have approved the use of PB for medical treatments under the trademark name Radiogardase®.[132,133] Indeed, the preferential exchange in favour of $Cs^+$ is linked to the fact that dehydrated $Cs^+$ cations perfectly accommodate the size of the PB tetrahedral sites. As the $Cs^+$ is a cation, which has a low affinity for water, its adsorption is preferential due to the confinement effect.[94] Theoretical studies have shown that the disorder of the position of compensating cations present in the pores is also strongly influenced by the presence and the organisation of the vacancies.[112] This latter also plays a role for the diffusion of large molecules or cations inside the pores. For instance, although the ion-exchange mechanism between alkaline ion implemented in the synthesis and $Cs^+$ has been the main adsorption mechanism, the high $Cs^+$ adsorption capacity might involve its migration through the vacancies for certain PBA compositions.[94] In this sense, it was also shown that lacunar PB exhibits a greater adsorption capacity with respect to non-lacunar structure. Such behaviour has been explained by the presence of hexacyanometallate vacancies, which engender a high number of coordinated and/or crystallizated water molecules. The proposed mechanism involves a proton elimination from a coordinated water on the iron sites to capture caesium and ensures the electroneutrality.[134]

Ionic exchange is also being largely used in the field of PB/PBA based batteries in which reversible insertion/deinsertion of alkaline ions may be achieved.[91,92,103] Moreover, recent studies have highlighted the possibility to use PBA to design ammonium-ion batteries storage by a simple PSM ion-exchange.[135] The $Na_{1.50}Ni[Fe(CN)_6]_{0.88}$ PBA could be for instance PSM modified by simply soaking the solid into an ammonium sulphate solution giving $(NH_4)_{1.47}Ni[Fe(CN)_6]_{0.88}$. This study clearly supports the possibility to adsorb small functional organic cation by ionic exchange.

### 3.2 Design of PB/PBA nanoparticles

Although PB is known since the 18th century, the synthesis of PB and PBA nanoparticles with size and shape control dates only shortly before the beginning of the new millennium. Different synthetic routes have been utilized to design nanoscale systems by constraining the growth of PBA crystals using for instance microemulsions,[136–138] ligands stabilization or polymer protection,[139–143] ionic liquids[144] or porous matrixes (silica,[145] chitosan[146] or alginates[147]). Such synthetic methods

 

have previously been described in several reviews and books.[4,7,8,10] In the scope of this overview, we will therefore focus on the synthetic routes allowing PB-type nanosystems to be used for their straightforward PSM.

Firstly, one of the most often used strategy for PB consists in the self-assembly reaction between two precursors, $Fe^{3+}$ and $[Fe(CN)_6]^{4-}$ (or $Fe^{2+}$ and $[Fe(CN)_6]^{3-}$), in water, in the presence of citrate ligands, which are attached at the surface as functional groups and prevented the nanoparticles agglomeration (Fig. 3A).[148] This method generally provides water-dispersible nanoparticles with the size varied from around ten to several tens of nanometers.[149–151] The coordinating ability of the citrate towards $Fe^{3+}$ ions appears to be the critical parameter to control the nucleation rate. This approach was also extended to other PBA.[151]

Secondly, another strategy particularly relevant for further PSM consists in the design of PB/PBA nanoparticles with a surface free of any stabilizers. Thus, PB nanoparticles without stabilizing agents were first prepared in 2002 by mixing $FeCl_3$ and $K_3[Fe(CN)_6]$ in the presence of the slight excess of $H_2O_2$ following by their self-assembly on a gold electrode (the average particles size was approximately of 50 nm).[152] The use of sonochemistry helps obtaining smaller PB nanoparticles with an average size of 5 nm.[153] Stable PB nanoparticles' suspensions were also obtained by mixing $K_3[Fe(CN)_6]$ and $FeCl_2$ with a large excess of the ferricyanide precursor (molar ratio 5 : 1).[154] They were then coated with a cationic polymer poly (ethylene imine) to design electrochromic thin films. A synthetic route based on potassium ferrocyanide as the single precursor was also published later,[155] by slow dissociation of $[Fe(CN)_6]^{4-}$ in the presence of hydrochloric acid. The particles size depends on the precursor concentration and the reaction temperature. In 2006, a major advance has been achieved by Brinzei *et al.* by taking advantage of the electrostatic stabilization of the PB colloids in water and in the absence of any stabilizing agents.[156] The controlled self-precipitation of the PBA precursors induces a negatively charged surface of the formed nanoparticles due to the presence of $[M'(CN)_6]^{p-}$ moieties. Starting from this, different research groups have optimized this method to obtain a large size and composition ranges of surfactant-free nanoparticles $M^{n+}/[M'(CN)_6]^{3-}$ (where $M^{n+}$ = $Ni^{2+}$, $Co^{2+}$, $Mn^{2+}$, $In^{3+}$, and $M'^{3+}$ = $Fe^{3+}$, $Cr^{3+}$).[156–161] For instance, the nanoparticle's size could be controlled from 6 to 200 nm by the simple modulation of the precursors' concentration and their addition rate (Fig. 3B–D).[158,162] Note that fast addition and high concentrations promote the nucleation process, which leads to the formation of small nanoparticles. In contrast, low concentrations and slow addition rate favour the growth of PBA nanocrystals, permitting accessing to large nanoparticles. Moreover, the presence of an excess of alkaline ions, such as $Cs^+$, favours the electrostatic stabilization and allows the formation of ultra-small (less than 10 nm) nanoparticles, as discussed by Catala *et al.*[10] Recently, the growth mechanism of mesoscale (100–500 nm) PBA particles was also investigated by Liang *et al.* A series of $Co^{2+}$ and $Ni^{2+}$ analogues, $Rb_jCo_k[M(CN)_6]_l{\cdot}nH_2O$ (M = Cr, Fe, Co) and $Rb_jNi_k[M(CN)_6]_l{\cdot}nH_2O$ (M = Cr, Fe, Co) are compared, along with the parent PB and the $Cu^{2+}$ analogue rubidium copper hexacyanoferrate.[163] While the $Cu^{2+}$ and $Ni^{2+}$ analogues grow by a traditional heterogeneous process, whereby nucleated particles grow by addition of ions from solution, $Co^{2+}$ analogues and rubidium PB nanoparticles grow by aggregation of precursor particles followed by annealing into crystalline mesoscale particles (Fig. 3E). Contrary to a common belief, such studies clearly point out the chemical-dependence of the size control of the PBA nanoparticles. This emphasizes the necessity to understand the underlying coordination chemistry's concepts in terms of stability/kinetics for the coordination complexes used during the synthesis.

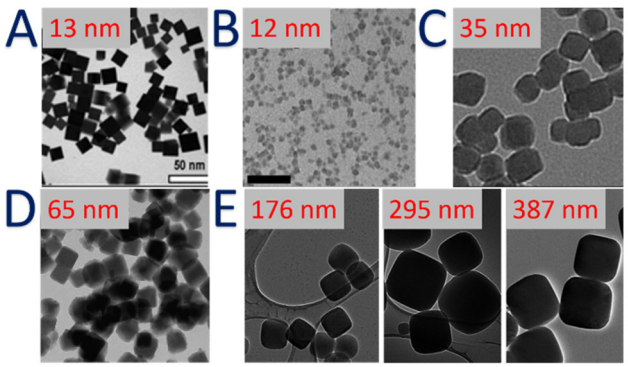


**Fig. 3** TEM images of: (A) citrate-stabilized PB nanoparticles. Reproduced from ref. 149 with permission from the Royal Society of Chemistry. (B) Self-standing charged $Cs_xNi[Cr(CN)_6]_y$ nanoparticles. Reproduced from ref. 165. Copyright 2014 Wiley-VCH Verlag GmbH & Co. KGaA, Weinheim. (C) Self-standing charged $K_xNi[Fe^{II}(CN)_6]_y$ nanoparticles. Reproduced from ref. 166 with permission from the Centre National de la Recherche Scientifique (CNRS) and the Royal Society of Chemistry. (D) Self-standing charged PB nanoparticles. Reprinted with permission from ref. 167. Copyright 2020 American Chemical Society. (E) Self-standing charged $K_xNi[Fe^{II}(CN)_6]_y$ nanoparticles. Reprinted with permission from ref. 163. Copyright 2020 American Chemical Society.

Self-standing charged PBA nanoparticles have opened the possibility to tune their size in a predictive way. For instance, alternative dropwise addition of molecular precursor solutions to a charged colloidal suspension of PBA "seeds" nanoparticles leads to a growth of these latter. This approach was applied to $Cs_{0.5}Ni[Cr(CN)_6]^{0.5-}$ under appropriate conditions in order to form the nanoparticles with the size ranging between 5 and 30 nm.[164] The obtained nanoparticles are not aggregated and well dispersed thanks to their surface charge high enough to ensure the electrostatic stabilization. Moreover, the influence of the growth conditions on the magnetic properties of such nanoparticles has also been explored.[164] Remarkably, the absence of a stabilizing agent on the nanoparticles surface makes them reactive due to the presence of $M^{n+}$ and $[M'(CN)_6]^{p-}$ groups.

This has been taken as an advantage to design more complex heterostructures, such as core@shell nanosystems with PBA of different chemical compositions combined with other inorganic materials (Au, $Fe_3O_4$, *etc.*).[168] Moreover, such

approach allows post-functionalizing either the particle's surface by various functional species depending on the targeted applications or the internalisation of targeted ions or molecules into the internal porosity of the coordination framework. This provides an efficient way to implement multifunctionality at the nanoscale without altering the core features (size, composition, intrinsic properties, *etc.*).

### 3.3 Hollow PB and PBA nanoparticles

Starting from the early of 2010's, the development of hollow nanostructures and related nano-frames has rapidly emerged for their potential applications in gas separation, alkaline-based batteries, catalysis, sensing, and drug delivery. The readers can refer to a recent review on this topic.[169] Hollow PB and PBA nanoparticles are usually larger than 10 nm and present a high external and especially internal surfaces. It is clear that these systems are not yet fully understood regarding the complexity of their chemical and physical properties, but the creation of a central void in the nanostructure coupled with the intrinsic microporosity of the PB/PBA shell might allow a better insertion and/or diffusion of molecules or ions. Moreover, the central void may also modify the physical properties of the nano-objects and in particular the magnetism.[170]

PB and PBA hollow particles have been synthesized using different strategies: the first approach based on the preparation of mini-emulsions, followed by a coordination polymerization at the periphery of the droplets has been reported by Liang *et al.*[171,172] A second route, more specific to PB, has been proposed by Zeng *et al.* based on the selective etching of already synthesised PB mesocrystals at high temperature in highly acidic conditions.[170,173,174] The chemical etching has now become the most popular strategy to design hollow PB structures and has been developed by other groups to prepare hollow PB and PBA nanoparticles of different size and composition (Fig. 4A).[169] Most of those have been prepared under acidic hydrothermal conditions (for example, by mixing the pristine nanoparticles with 1 M HCl solution in a Teflon vessel at 140 °C for 20 h; Fig. 4B).[170,175,176] The PVP located at the surface particles prevent the surface etching, while the acid can easily diffuse within the porosity of the PB or PBA framework to dissolve the core. Another etching process based on the use of ammonia has also been applied to $Ni^{2+}/[Co(CN)_6]^{3-}$ nanoparticles (Fig. 4C).[177] However, it is important to emphasize that the chemical etching is highly dependent on the chemical composition of PBA and in turn on the chemical stability of the M′–CN–M linkages. Thus, the formation of different complex architectures could be observed (hollow nanocubes, nano-frames, nanocages, Fig. 4).[169] This approach also raises problems concerning the kinetic control of the etching.

Thirdly, a different etching strategy to design hollow systems has been developed by using core@shell heterostructure. Risset *et al.* designed core@shell PBA@PBA′ heterostructures with a potentially "soluble" $Rb_{1.6}Mn_4[Fe(CN)_6]_{3.2}\cdot 4.8H_2O$ core and $Rb_{0.4}M_4[Fe(CN)_6]_{2.8}\cdot 7.2H_2O$ (M = Co, Ni) as a shell. The "soluble" $Rb_{1.6}Mn_4[Fe(CN)_6]_{3.2}\cdot 4.8H_2O$ compound exhibits weak Fe–CN–Mn linkages that could be broken by an extensive washing, leading to $Rb_{0.4}M_4[Fe(CN)_6]_{2.8}\cdot 7.2H_2O$ PBA hollow nanoparticles of 10 nm thickness (Fig. 4D).[178] Our group reported also an alternative approach starting from $Au@K_{1.20}Ni^{II}[Fe^{II}(CN)_6]_{0.80}$ core@shell nanoparticles.[179] Metallic gold could be post-synthetically dissolved in the presence of cyanide ions and oxygen, thanks to the high stability constant of the gold cyanide complex, $[Au(CN)_2]^-$ ($10^{37}$ $M^{-2}$). By taking advantage of the intrinsic porosity of the PBA network, hollow PBA nanoparticles can be obtained by simply dispersing the core–shell $Au@K_{1.20}Ni^{II}[Fe^{II}(CN)_6]_{0.80}$ nanoparticles in a dilute KCN solution without affecting the integrity of the $K_{1.20}Ni^{II}[Fe^{II}(CN)_6]_{0.80}$ cyano-bridged shell. Since the shell thickness could be easily adjusted, the $CN^-$ diffusion in the porosity of the cyano-bridged framework could allow obtaining of tuneable hollow systems (Fig. 4E).[179] Recently, other etching approaches using sodium tungstate have also been used to design hollow PB and cobalt hexacyanoferrate

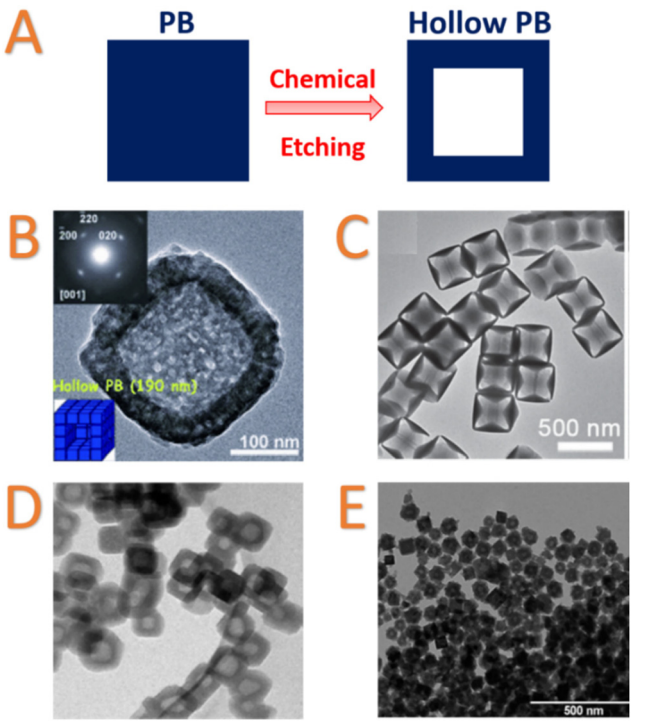


**Fig. 4** (A) Schematic Representation of chemical etching to prepare hollow nanoparticles; TEM images of: (B) hollow PB mesocrystals synthesized by chemical HCl etching. Inset: Selected-area electron diffraction patterns of one particle. Reproduced from ref. 170. Copyright 2012 Wiley-VCH Verlag GmbH & Co. KGaA, Weinheim; (C) etching product obtained after reacting of $Ni^{2+}/[Co(CN)_6]^{3-}$ PBA nanocubes with ammonia at room temperature for 6 h. Reproduced from ref. 177. Copyright 2016 Wiley-VCH Verlag GmbH & Co. KGaA, Weinheim; (D) hollow nanocubes of $Rb_{0.4}Co_4[Fe(CN)_6]_{2.8}\cdot 7.2H_2O$ with $Ni_x[Cr(CN)_6]_y$ deposit on the surface. Scale bar = 200 nm. Reprinted with permission from ref. 178. Copyright 2013 American Chemical Society; (E) hollow $KNi[Fe(CN)_6]$ nanoparticles after etching of gold core. Reproduced from ref. 179. Copyright 2014 Wiley-VCH Verlag GmbH & Co. KGaA, Weinheim.

nanoparticles.[180] In the last case, the *in situ* etching during the synthesis could be controlled by modulation of the Fe/Co ratio and stirring time, which affect the dissolution/recrystallization process. Employing a complementary approach that was used for Au@PBA core@shell structures, a self-templating synthesis of cobalt hexacyanoferrate hollow structures with controllable morphologies has been proposed.[181] Cobalt-hexacyanoferrate nano-objects of different morphologies (spheres, polyhedrons, prisms) were prepared. Dispersion in water induces the dissolution of $Co^{2+}$ ions that could subsequently react with hexacyanoferrate to yield the hollow nanostructures.

Considerable efforts have been devoted to explore the field of hollow nanoparticles. However, for future applications, a generalized method that can produce PB and PBA hollow structures with controllable size, shell thickness and in large scale has still to be developed.

# 4 Post-synthetic modification (PSM) of Prussian blue type nanoparticles

## 4.1 Generalities and mechanisms

After a brief description of essential features of PB and PBA nanomaterials, it appears that both, nanochemistry and molecular chemistry concepts, could be applied for the PSM of PB/PBA nanoparticles when they present the appropriate functional groups or active metal centres on their surface and/or inside the internal porosity. Thus, and like their MOF counterpart, both the surface and the internal porosity of PB/PBA may be post-functionalized.

## 4.2 Surface functionalization

The possibility to modify the PB nanoparticles' surface has been very recently reviewed in the scope of biomedical applications.[12] Consequently, we will emphasize herein the different synthetic strategies involving various interactions between the nanoparticles' surface and targeted organic species to achieve surface PSM by giving some representative examples from the literature (Table 1).

(i) *Surface ligand exchange*. When the synthesis of nanoparticles is achieved using stabilizing agent, the ligands coordinated to the metal ions situated on the nanoparticle surface could be exchanged by stronger ones. Hence, the first post-synthetic ligand exchange has been achieved in the beginning of the 2000's in the case of cobalt hexacyanoferrate and hexacyanochromate nanoparticles by substituting weakly-bonded ligands by aliphatic amines.[137] In this work, the nanoparticles were firstly synthesized by a reverse micelle technique using poly-(ethylene glycol) mono 4-nonylphenyl ether (NP-5). A long aliphatic amine (stearylamine) was subsequently exchanged as primary amines are stronger donors than oxygens towards transition metal ions situated on the surface, such as $Co^{2+}$. This surface modification allows the nanoparticles to change their dispersibility in less polar solvents.

(ii) *Direct post synthetic functionalization of stabilising agent-free nanoparticles*. Both, the Lewis-acid character of $M^{n+}$ ions and the Lewis-base character of the $[M'(CN)_6]^{p-}$ moieties situated on the nanoparticle surface could be utilized in this purpose. On the one hand, suitable ligands presenting available coordinative functions (amine or carboxylate) can substitute the water molecules completing the coordination sphere of surface metallic ions, $M^{n+}$, and interact by coordinative bonds with these surface exposed metal ions (Fig. 5).[182,183] For instance, as-isolated undispersible (in water or organic solvents) nanoparticles of PB, nickel and cobalt hexacyanoferrate PBA of 10–20 nm diameter were post-functionalized with oleylamine to afford their good dispersibility in usual organic solvents (Fig. 7A).[182] On the other hand, the post-synthetic addition using an "inorganic ligand", such as $[Fe(CN)_6]^{4-}$, also provides their hydrodispersibility by coordination of $[Fe(CN)_6]^{4-}$ to the $M^{n+}$ active site. Yet, simple electrostatic stabilization of the nanoparticles by negatively charged hexacyanoferrate could not be excluded. In both cases, the resulting surface negative charge allows the stabilization of the nanoparticles in water. Dual surface modification with both, $[Fe(CN)_6]^{4-}$ and various alkylamines ($C_3$ to $C_{18}$), was later utilized to render surfactant-free PB nanoparticles of 10 nm dispersible in alcohols.[183] A mechanism proposed by the authors explaining the appearance of a surface negative charge is based on the acid/base reaction involving the coordinated water molecules of the $Fe(OH_2)$ sites and the amine function. The possibility to synthesize size-controllable negatively charged particles dispersible in polar solvents without any stabilizers greatly extends the post-functionalization approaches. For instance, nickel hexacyanoferrate nanoparticles with size ranging from 40 to 100 nm could undergo PSM by a PEG exhibiting terminal amine functions allowing its attachment at the surface of the particles through a coordination bond with the surface-exposed $Ni^{2+}$ ions. This surface modification allows to compare the PBA nanoparticles of different sizes and establish the impact of the nanoparticles size on their Debye temperature.[162]

Another example showing the ability of the reactive surface sites of PB/PBA nanoparticles to establish strong coordination bonds concerns the two-steps PSM of PVP-stabilized nanoparticles. Despite the presence of PVP, which could potentially restrain the surface accessibility, the cyano groups of the surface act as Lewis basic sites for the coordination of iron pentacarbonyl, $[Fe(CO)_5]$, as confirmed by the change in the PB nanoparticles zeta potential and XPS analysis.[184] Remarkably, the nanoparticles could be afterwards reacted with an amine functionalized PEG by coordination with the Lewis acid iron ions at the surface. Such result clearly highlights the intrinsic dual Lewis acid/base character of the PB/PBA surface.

(iii) *Post-synthetic coating* could also be achieved using electrostatic or weak interactions. As previously stated, PB/PBA nanoparticles could exhibit negative surface charge that arises either from the presence of stabilizing agents, such as for instance citrates, or the presence of hexacyanometallate moieties. Caesium nickel hexacyanochromate was modified using a cationic surfactant, such as cetyl trimethyl ammonium chlor-

**Table 1** Surface functionalization of PB/PBA nanoparticles

| Nanoparticle formula | Nanoparticle synthesis (surface stabilizing agent) | Method | Chemical species used for PSM | Benefit of PSM | Application | Ref. |
|---|---|---|---|---|---|---|
| $Co_x[M^{III}(CN)_6]_y$ (M = $Cr^{III}$, $Fe^{III}$) | Reverse micelle (NP-5) | Organic ligand exchange; polymer coating or displacement | Stearylamine | Nanoparticles' stability | Fundamental study | 137 |
| $K_{1-3x}Gd_xFe[Fe(CN)_6]$ | PVP-coated nanoparticles | | PEG | Stability in physiological media | MRI contrast agents with stability in an acidic environment | 193 |
| $K_xFe_y[Fe(CN)_6]_z$ | PVP-coated nanoparticles | | Hyaluronic acid grafting polyethylene glycol (HA-*g*-PEG) and loading with 10-hydroxycamptothecin | Stability in the physiological conditions and long blood circulation | Photo/chemo thermal agent for cancer therapy | 194 |
| $K_xFe_y[Fe(CN)_6]_z$ doped with $Mn^{2+}$ | Hydrothermal reaction in the presence of PVP | | Doxorubicin followed by red blood cell | Stability in the physiological conditions and long blood circulation | Photo/chemo cancer therapy | 195 |
| $K_xFe_y[Fe(CN)_6]_z$ | Citrate-stabilized nanoparticles | | 3 polymer shells: (1) polyallylamine hydrochloride; (2) anionic poly (acrylic acid); (3) amine terminated PEG | Stability in physiological media | Cancer imaging and photothermal therapy | 189 |
| $K_xFe_y[Fe(CN)_6]_z$ doped with $Mn^{2+}$ | | | | | Bimodal MRI/Photoacoustic Imaging and Photothermal Therapy | 190 |
| $K_xFe_y[Fe(CN)_6]_z$ | | | Dopamine followed by human-serum albumin and doxorubicin | Stability in physiological media | pH —/thermotriggered drug-delivery | 196 |
| $K_xFe_y[Fe(CN)_6]_z$ | | | Dopamine followed by bi-amino PEG and folic acid | Biocompatibility, tumor targeting | MRI agent and chemo/ photothermal therapy | 197 |
| $Fe_3O_4@K_xFe_y[Fe(CN)_6]_z$ | Self-standing charged nanoparticles | Direct functionalization (coordination bond) | Dopamine followed by bovine-serum albumin and aluminum phthalocyanine | Biocompatibility; prolongation of circulatory half-life; second-generation photosensitizer and fluorescence imaging | NIR/magnetic resonance/ photoacoustic imaging and photothermal/ photodynamic therapy | 198 |
| $Fe_4[Fe(CN)_6]_3{\cdot}15H_2O$, $Co_{1.5}[Fe(CN)_6]$, $Ni_{1.5}[Fe(CN)_6]$ | | | Oleylamine $[Fe(CN)_6]^{4-}$ | Organic solvent dispersion Water dispersion | Organic or water dispersible inks | 182 |
| $Fe_4[Fe(CN)_6]_3{\cdot}15H_2O$ | | | Alkylamines ($C_3$-, $C_4$-, $C_6$-, $C_8$-, $C_{12}$-, $C_{16}$-, $C_{18}$-) | Water and alcohols dispersion | Realisation of printed electronics | 183 |
| $K_xFe_y[Fe(CN)_6]_z$ | | | $[Fe(CN)_6]^{4-}$ followed by alkylamines $[Fe(CO)_5]$ | CO release | Photo/chemo thermal agent for cancer therapy | 184 |
| | | | Amine-terminated PEG | Better blood circulation period | | |
| $Fe_4[Fe(CN)_6]_3{\cdot}15H_2O$ | | | Oleylamine followed by lipid-PEGylation with doxorubicin in the lipid. | Stability in physiological media; Drug delivery | pH-responsive drug carriers for Photo/Chemo cancer therapy | 191 |
| $Fe_3O_4@K_xFe_y[Fe(CN)_6]_z$ | | | Oleylamine-PEG/lipid, doxorubicin | Interfacial biocompatibility and stability of nanoparticle; drug delivery | Photo/chemo thermal agent for cancer therapy | 199 |
| $Ni_x[Fe^{III}(CN)_6]_y$ | | | Toluidine blue | Electron transfer mediator | Electrochemical immunosensor | 200 |
| $K_xFe_y[Fe(CN)_6]_z$ | | | Carboxyl fluorescein modified ssDNA and cyanine 5 modified ss DNA | Fluorescence imaging | Nanoprobes for microRNA detection | 201 |

**Table 1** *(Contd.)*

| Nanoparticle formula | Nanoparticle synthesis (surface stabilizing agent) | Method | Chemical species used for PSM | Benefit of PSM | Application | Ref. |
|---|---|---|---|---|---|---|
| $Cs_xNi[Cr(CN)_6]_y$ | Self-standing charged nanoparticles | Direct functionalization (electrostatic or weak interactions) | Cetyl trimethyl ammonium chloride PVP | Nanoparticles' isolation in powder form | Magnetic properties study | 156 |
| $K_{4y-3+x}Mn^{II}{}_xIn^{III}{}_{1-x}[Fe^{II}(CN)_6]_y$ | | | Dextran | Nanoparticles' stability | T1 contrast agents for magnetic resonance imaging | 161 |
| $Na_{0.10}Fe[Fe(CN)_6]_{0.77}$ | | | Dextran<br>Lipid bilayers | Nanoparticles' stability, biocompatibility | Nanoprobes for SPEC-CT imaging | 185 |
| $K_{0.53}Gd_{0.89}Fe^{III}{}_4[Fe^{II}(CN)_6]_{3.8}\cdot 1.2H_2O$ | | | Avidin-Alexa Fluor 488, anti-human eotaxin-3 antibody | Fluorescence targeting | Multimodal molecular imaging agent | 202 |
| $K_{0.6}Mn_{0.7}Fe^{III}{}_4[Fe^{II}(CN)_6]_{3.5}\cdot 3H_2O$ | | | Avidin-Alexa Fluor 488, anti-neuron-glial antigen 2, Eotaxin-3 antibody, biotinylated human transferrin | | Imaging of pediatric brain tumors | 203 |
| $K_xFe_y[Fe(CN)_6]_z$ | | | Avidin-Alexa Fluor 488, antigen-specific cytotoxic T lymphocites | Immunotherapy | Photothermal therapy for cancer treatment | 192 |
| $Ni_x[Fe^{III}(CN)_6]_y$ | | | 7,7,8,8-Tetracyanoquinododimethane | Electron acceptor | Host material for sodium ion storage | 204 |
| $Fe_3O_4@K_xFe_y[Fe(CN)_6]@CuInS_2–ZnS$ | | | Polyethyleneimine | Coupling agent | Coupling with quantum dots nanoparticles for dual fluorescence/MRI imaging and photothermal therapy | 205 |
| $Na_{0.30}Fe^{III}[Fe^{II}(CN)_6]_{0.82}\cdot 3.7H_2O$ | | | Rhodamine B | Fluorescence imaging | *In vitro* fluorescence imaging | 167 |
| $K_xFe_y[Fe(CN)_6]_z$ | Chitosan-stabilized nanoparticles | | DNA | Gene delivery | Photothermally enhanced gene delivery | 206 |
| $K_xFe_y[Fe(CN)_6]_z$ | Citrate-stabilized nanoparticles | | Poly-L-lysine | Improve cell internalization | Photoacoustic imaging of human mesenchymal stem cells | 186 |
| $K_xFe_y[Fe(CN)_6]_z$ | PVP-stabilized nanoparticles | | 11-Mercaptoundecanoic acid | Coupling agent for DNA drugs | DNA drug delivery | 188 |
| $K_xFe_y[Fe(CN)_6]_z$ | Citrate-stabilized nanoparticles | Ligand conjugation | 5-(Aminoacetamido)fluorescein | Fluorescence | MRI and confocal imaging | 150 |
| $K_xFe_y[Fe(CN)_6]_z$ | | | Texas red | Fluorescence marker | Cellular imaging and drug delivery | 149 |
| $K_xFe_y[Fe(CN)_6]_z$ | | | Glypican-3 antibodies | Tumor targeting | Targeted imaging and therapy | 207 |
| $K_xFe_y[Fe(CN)_6]_z$ | | | Folic acid | Nanoparticles' stability and binding affinity for cancer cells | Electrochemical detection of targeted cancer cells | 208 |
| $K_xFe_y[Fe(CN)_6]_z$ | | | Methylene blue | Fluorescence | Optical imaging | 209 |
| $K_xFe_y[Fe(CN)_6]_z$ | Human serum-albumin stabilized nanoparticles | | Indocyanine green | Fluorescence imaging | Bimodal imaging | 210 |

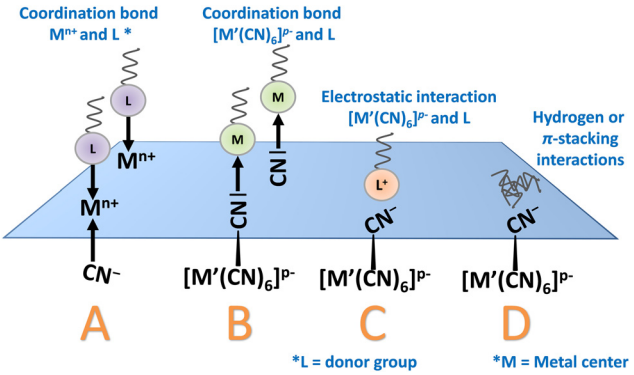


**Fig. 5** Schematic representation of different interactions between ligands and PB/PBA nanoparticles: (A) coordination bond between $M^{n+}$ ions and donor group (L); (B) coordination bond between $[M'(CN)_6]^{p-}$ and M; (C) electrostatic interaction between $[M'(CN)_6]^{p-}$ and L; (D) hydrogen or π-stacking interactions between cyano-groups and ligands.

ide, that would interact with the negatively charged surface through electrostatic interactions. On the other hand, PVP, able to weaky coordinate nickel ions at the surface, could be post-synthetically introduced.[156] Other stabilizing agents, such as biopolymer dextran[161,185] or lipid bilayers,[185] were also employed to post-synthetically functionalize the surface of PB/PBA nanoparticles through the formation of weak bonds or electrostatic interactions. Other example concerns citrate-stabilized PB nanoparticles of 50–60 nm that could be complexed with cationic transfection agent poly-L-lysine *via* electrostatic interactions.[186]

(iv) *Coupling reactions using the stabilizer attached at the surface of the PB nanoparticles*. As an example, a fluorescein-based dye bearing an amine function was conjugated to citrate coated-nanoparticles by a classical coupling reaction between carboxylic acid and amines involving 1-ethyl-3-(3-dimethylaminopropyl)carbodiimide (EDC) to implement luminescence for *in vitro* fluorescence imaging.[187] The same strategy was also applied with the Texas red dye.[149] PVP-stabilized nanoparticles could be functionalized by 11-mercaptoundecanoic acid (DUA) for subsequent amino or thiol-based DNA drug conjugation through EDC/NHS chemistry and/or oxidative disulfide bond linkage to allow the DNA drug delivery in cancer cells.[188] Multi-steps surface functionalization could also be performed to achieve a layer-by-layer coating.[189–191] For example, citrate-stabilized PB nanoparticles react with a cationic polymer (polyaniline hydrochloride) and then with the polyacrylic acid anionic polymer through electrostatic interactions and by EDC coupling, respectively.[189] An amine terminated PEG is then conjugated with the carboxyl groups through amide formation. Another example concerns stabilising agent-free nanoparticles of PB that could be firstly functionalized with avidine through electrostatic interactions before conjugation, which could be achieved by reaction with biotin using the strong avidin–biotin interaction.[192] The resulting functionalized PB nanoparticles could be then attached with antigen-specific cytotoxic T lymphocites (CTL).

Naturally, all the available chemical interactions could be combined using multistep surface functionalization (Table 1) in order to finely adjust the physico-chemical properties and/or pharmacokinetic features.

To give an example, PB nanoparticles could be first post-functionalized with oleylamine (coordination bond) and subsequently with a PEG-based lipid through a thin-film hydration process to give hydrophilic PEGylated nanoparticles.[191] The diversity in the surface interactions results in a chemical "toolbox" that provides numerous strategies for the PSM of the PB/PBA surface. Most of these studies rely on the nanoparticle tailoring for biomedical applications (*e.g.* bio-imaging or cancer treatments) that would be detailed in the next part.

### 4.3 Adsorption within the PB/PBA internal porosity

In a similar manner than for MOF, the porous character of PB/PBA nanoparticles could be utilized for the PSM. Nevertheless, and in contrast to MOF, the linkers used for the synthesis of PB/PBA (hexacyanometallate complexes) could hardly be functionalized through introduction of chemical functions to perform PSM. To our knowledge, no post-functionalization of PB and PBA nanoparticles within the internal porosity of the cyano-bridged framework until the beginning of the 2010's has been reported, although the adsorption of guest molecules is one of the most powerful strategies applied to MOF.[48,49,55,222] As previously mentioned, the presence of hexacyanometallate vacancies creates pores that could reach up to a diameter of 7.5 Å for single vacancies and even larger in case of adjacent double vacancies. As we will describe *vide infra*, these pores could engender different types of interactions of various nature and strength (Fig. 6 and Table 2) with potential guests.

Firstly, the presence of water molecules coordinated on the metal ion located in the vicinity of hexacyanometallate vacancies gives rise to the presence of reactive metal ion sites with an average chemical environment $[M(NC)_4(H_2O)_2]$.

The labile coordinated water molecules could be easily substituted by stronger ligands or simply removed by thermal activation to afford coordinatively unsaturated site. As a consequence, a suitable guest presenting an appropriate Lewis base character would be able to react on these acid sites through a chemisorption process. In the scope of PBA nanoparticles, this methodology appears quite unexplored and has been only recently applied to PB and nickel hexacyanoferrate nanoparticles functionalized by the 2-aminoanthracene luminophore, which is able to enter into the porosity and presents an amine function able to substitute water molecules.[167,223] In addition, alkaline ions may be present in the tetrahedral sites of the PB/PBA structure and can be exchanged with another cation of the appropriate size and charge. As previously stated, these guest cations could readily diffuse into the porous structure for ionic exchange. As an example, PB nanoparticles possessing $Na^+$ in their framework have been used for improved $Cs^+$ elimination from living organisms. In this case, the use of PB nanoparticles presents the advantage to enhance the $Cs^+$

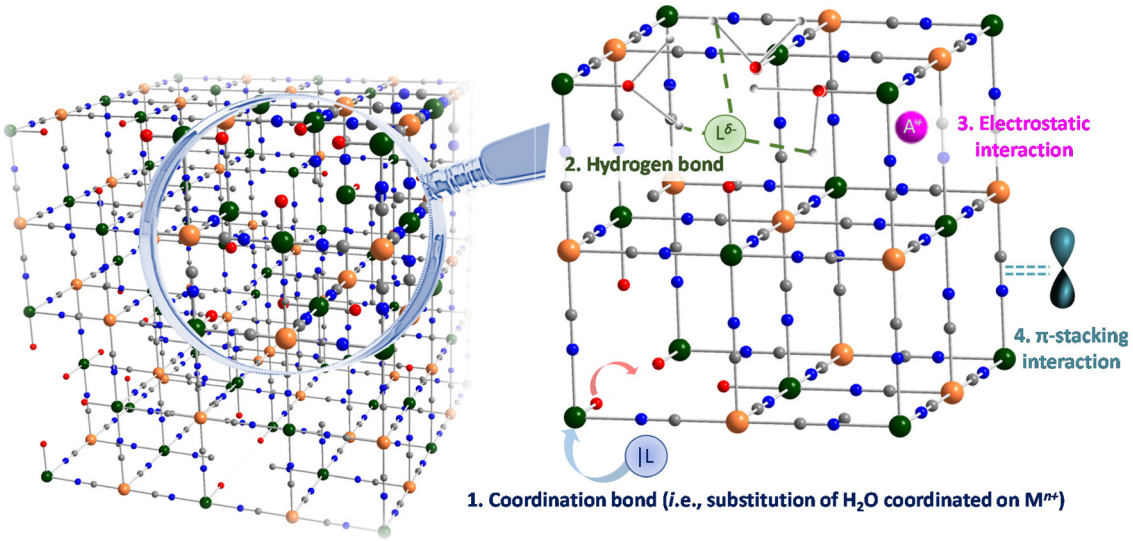


**Fig. 6** Schematic representation of different interactions in the PBA structures.

**Table 2** Loading in porous PB or PBA nanoparticles

| Nanoparticle formula | Porosity type | Guest | Interaction guest-framework | Application | Ref. |
|---|---|---|---|---|---|
| $K_xFe_y[Fe(CN)_6]_z$ | Hollow nanoparticles | Cisplatin | Not discussed | Intracellular drug delivery | 211 |
| $K_xFe_y[Fe(CN)_6]_z$ | | Doxorubicin | Electrostatic interaction (negative PB–positive DOX) or coordinative bonding between Fe(III) and amino or carbonyl groups of DOX | Chemo-thermal tumor therapy | 212 |
| | | Perfluoropentane | Not discussed | | |
| $K_xFe_y[Fe(CN)_6]_z$ | | Doxorubicin | π-stacking or hydrophobic | Chemotherapy against hepatocellular carcinoma | 213 |
| $K_xFe_y[Fe(CN)_6]_z$ | | Doxorubicin | Interaction between Fe(III) and DOX | Chemotherapy of cancer | 214 |
| $K_xFe_y[Fe(CN)_6]_z$ | | Chloroquine, 1-tetradecanol | Not discussed | Autophagy inhibition and cancer treatment | 215 |
| $K_xFe_y[Fe(CN)_6]_z$ | | 1-Tetradecanol, Doxorubicin, camptothecin | Not discussed | NIR light responsive drug co-delivery system | 216 |
| $K_xFe_y[Fe(CN)_6]_z$ | | 1-Pentadecanol, Doxorubicin | Not discussed | NIR-induced chemo-photothermal tumor therapy with trimodal imaging | 217 |
| $Na_{0.45}Fe[Fe(CN)_6]_{0.86}$@(PEG–$NH_2$)$_{0.22}$ | Tetrahedral sites | $^{201}Tl^+$ | Electrostatic interactions | Nano-radiotracers for SPECT imaging | 218 |
| $Na_{0.10}Fe[Fe(CN)_6]_{0.77}$ | | $^{201}Tl^+$ | Electrostatic interactions | Nano-radiotracers for SPECT imaging | 185 |
| $K_{0.04}Ni[Cr(CN)_6]_{0.64}\cdot 4.1H_2O$ | Hexacyanometallate vacancies | 2-Aminoanthracene (AA) | Coordinative bonds between Ni(II) and amino group of AA | Luminescent NPs | 219 |
| $Na_{0.30}Fe^{III}[Fe^{II}(CN)_6]_{0.82}\cdot 3.7H_2O$ | | 2-Aminoanthracene (AA) | Coordinative bonds between Fe(III) and amino group of AA | *In vitro* imaging | 167 |

adsorption kinetics and change the $Cs^+$ elimination way (glomerular *vs.* faeces).[224]

These PSM methodologies could also be applied to hollow PB nanoparticles (Fig. 7B and Table 2) by taking advantage of the large voids accessible in the internal cavity of the nanostructure.[194,211–213] Hence, hollow nanoparticles appear to be efficient carriers for therapeutic molecules with applications in drug delivery (see the next section). However, we would like to emphasize that there is, for the moment, only little information about the encapsulation process of the drugs in the nanoparticle cavities and their interaction with the coordination network. Since these nanoparticles are mostly obtained by an etching process, the PB/PBA nanoparticles most likely exhibit larger voids caused by defects with respect

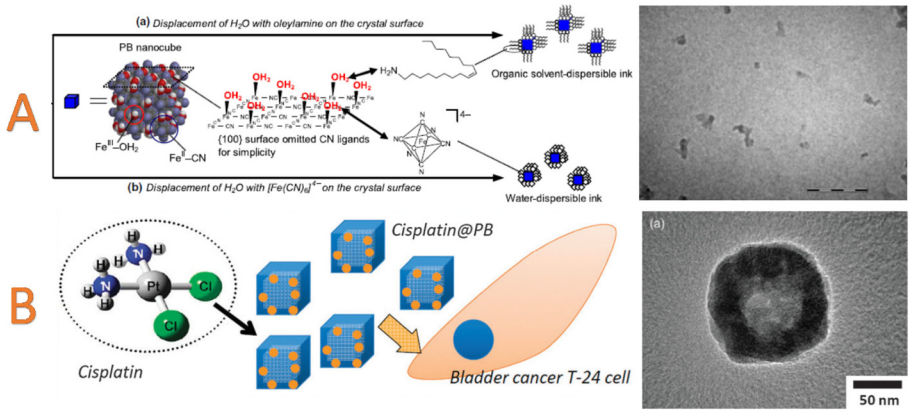


**Fig. 7** (A) Schematic representation of PB nanoparticles inks. The surface modification with oleylamine leads to organic-solvent dispersible PB pigment. TEM image of PB nanoparticles in the toluene-dispersible ink. Scale bar = 100 nm. Reproduced with permission from ref. 182. © IOP Publishing. All rights reserved. (B) Schematic representation of hollow PB nanoparticles loading with cisplatin. TEM image of cisplatin@hollow PB. Reproduced from ref. 211 with permission from the Royal Society of Chemistry.

to non-hollow ones. To finish, the loading within the porosity could be combined with the nanoparticles' surface modification. Such few examples are grouped in Table 3.

## 5 Towards multifunctional PB/PBA nanoparticles by PSM

### 5.1 Drug delivery, photothermal therapy and PSM

One of the main motivations in the design and studies of nano-sized PB concerns their use for biomedical applications. This fact could be explained by the exceptional physico-chemical features of PB and its biocompatibility. Firstly, it exhibits a very high stability (dissociation constant for the bulk PB compound is equal to $3 \times 10^{-41}$) in acidic/neutral media. Moreover, the biocompatible character of PB has been validated in its bulk form by the Food and Drug Administration (FDA) as an antidote for a $Cs^+$ or $Tl^+$ empoisoning for human being.[132,133] In the scope of this article, we will not detail all the biomedical applications, which have already been discussed in dedicated reviews.[5,9–11] A focus will be given here to demonstrate how the PSM approach could be used to tailor and bring additional tools for such targeted applications. In a nutshell, the efficiency of nanosized PB has been demonstrated for Magnetic Resonance Imaging (MRI),[140,149,150,161,190,202,203,225–230] scintigraphy,[218] photo-acoustic imaging,[231,232] therapy through different kinds of treatment[233,234] including drug delivery[211,233–236] and photothermal therapy.[190,215,220,229,237–242] For the latter, high absorption of PB in the Near InfraRed (NIR) spectral domain (650–900 nm) and high light-to-heat conversion efficiency have been explored for the design of potential laser-assisted photothermal ablation agents for cancer therapy, which could also concomitantly trigger the drug delivery.

In the scope of PSM, the ion capture of radioactive $^{201}Tl$-labeled in ultra-small[218] or larger PB nanoparticles[185] have been designed for their employment as radiotracers for Single-Photon Emission Computed Tomography (SPECT) imaging. PB nanoparticles of 2–3 nm have been synthesized with different coatings by biocompatible ligands (glycol chains and/or carbohydrates). These later are covalently anchored *via* functional amino groups at the nanoparticles surface allowing an excellent colloidal stability in physiological solutions and a prolonged blood circulation. The PSM is carried out by simply reacting the nanoparticles with small amount of radioactive thallium isotopes ($^{201}Tl^+$) that were irreversibly trapped in the tetrahedral sites of the PB structure due to their appropriate size. In contrast to the commercial $^{201}TlCl$, which is commonly used as radiotracer for the scintigraphy of heart and which in majority accumulates in the kidney within a few minutes after

**Table 3** Surface modification and loading within porosity

| Nanoparticle formula | Porosity type | Guest | Interaction guest-framework | Application | Ref. |
|---|---|---|---|---|---|
| $K_xFe_y[Fe(CN)_6]_z$ modified with polyethyleneimine | Hollow nanoparticles | Indocyanine green, Doxorubicin | Electrostatic interaction | Fluorescence-guided tri-modal combination therapy of cancer | 220 |
| $K_xFe_y[Fe(CN)_6]_z$ surface modified with hyaluronic acid grafting polyethylene glycol | Hollow nanoparticles | 10-Hydroxycamptothecin | Not discussed | Thermochemotherapy of cancer | 194 |
| $Na_{0.38}Mn_{0.12}Fe[Fe(CN)_6]_{0.91}$ | Solid nanoparticles with microporosity | Doxorubicin | Weak interactions | Photothermal therapy and drug delivery | 221 |

 

injection, the functionalized nanoparticles might act as radiotracers for the scintigraphy of lungs and liver.

One of the main routes to perform PSM for biomedical applications consists in the possibility to encapsulate different drugs in the PB nanoparticles and in the related hollow architectures. The combination of the photothermal therapy with the drug delivery based on the PB type nanocarriers enhances the cancer cell killing activity.[211,235,243] Before going into some relevant examples, it should be emphasized that the quantitative comparison between different studies in terms of loading capacity and/or loading efficiency appears relatively difficult due to the absence of strict definition (initial weight of nanoparticles or total weight of nanoparticles, consideration of solvent molecules *etc*.) to calculate these features The first loading of a drug into PB could be traced back in 2012 by Lian *et al.* in hollow nanoparticles protected by PVP.[211] The anticancerous agent cisplatin *cis*-$[Pt(NH_3)_2Cl_2]$ complex was simply loaded by immersion into an aqueous suspension of PB nanoparticles (Fig. 7B). The loading efficiency was reported to be almost 100%, whereas the proposed mechanism indicates that the cisplatin was loaded into the microporosity of the PB coordination framework by considering a comparable size between the coordination complex guest and the PB pores. Consequently, the large pore of the hollow nano-architecture was apparently not involved in the adsorption mechanism of the drug (even if it can play a role in the diffusion of the molecules in order to reach the microporosity). The resulting loaded nano-objects have been utilized as an anticancer drug on bladder cancer T24 cells, confirming its therapeutic effect.

It was also later suggested that drugs of greater size, such as doxorubicin (DOX), could be adsorbed in both, PB and hollow PB nanoparticles. This subject was largely studied in the literature (Tables 1–3) and mainly in hollow nanoparticles, and it appears that DOX can be captured in the large porosity of PB or attached at the surface of particles. For instance, a drug loading efficiency of 98% was achieved in hollow PB nanoparticles.[212] The authors ascribed such high loading efficiency to the presence of numerous mesopores and a huge cavity in the case of hollow particles, as well as to the formation of electrostatic interactions and/or coordination bonds involving the DOX amino, carbonyl or hydroxyl groups with the surface. The release of the loaded DOX could be triggered at low pH values. Remarkably, the thermosensitive phase change material perfluoropentane could be subsequently loaded into the previously functionalized PB/DOX nanoparticles to enhance the ultrasound contrast upon irradiation. The obtained nanosystems exhibit a synergistic effect in the chemo-thermal therapy. In another study, a loading content of 33 wt% and a loading efficiency of 88 wt% was also reported for hollow PB nanoparticles.[213] In that case, the authors suggest that the loading of DOX relies on π stacking and hydrophobic interactions into the interior cavity. Remarkably, co-adsorption could also be achieved using DOX and another drug (camptothecin) in hollow PB nanoparticles in association with an introduction of a phase-change material (1-tetradecanol, melting point = 38 °C), the latter acting as both, a thermosensitive gatekeeper and a medium for loading hydrophilic and hydrophobic drugs.[216] The NIR light treatment provides a precise light triggered co-delivery of DOX and camptothecin. A closely related example has also been reported using 1-pentadecanol as a phase change material and DOX in hollow PB particles of 130 nm that were obtained from polystyrene nanoparticles as a template.[217] Another example consists in the demonstration of the fluorophore (indocyanine green) and DOX entrapment at the surface and possibly within the interior cavity of polyethyleneimine-modified hollow PB nanostructures.[220] The surface charge modification using polyethyleneimine affords a nanoparticles' positive surface charge that allows the subsequent interaction with the anionic indocyanine green molecules at the surface. Then, electrostatic interactions between DOX and indocyanine are responsible for the DOX capture. Despite the fact that the localization of DOX was not clearly demonstrated, such example proves the efficiency of the step-by-step (or layer-by-layer) PSM surface modification. The drug loading efficiency for indocyanine green and DOX was calculated as 5.85% and 6.74%, respectively, while the encapsulation efficiency was estimated at 40% and 32%. The systems could be viewed as a triple-modal combination therapy with photothermal and photodynamic effects associated with a drug release.

In addition to the aforementioned examples of co-drugs or dyes loading, other pharmaceutical guests could be post-synthetically adsorbed. Hence, 10-hydroxycamptothecin, a chemotherapeutic agent, has been successfully adsorbed in hyaluronic acid/PEG modified hollow PB nanoparticles obtained by layer-by-layer surface modification.[194] The loading capacity of 10.4% and an encapsulation efficiency of 52% of 10-hydroxycamptothecin suggests its loading in the internal mesopore. Both, *in vitro* and *in vivo* experiments confirm its slow release as well as the possibility of photothermally-assisted drug release. Also, chloroquine, which is an autophagy inhibitor, has been simultaneously loaded with a phase-changing material (1-tetradecanol) in hollow PB nanoparticles.[215] Both molecules are located in the interior cavity of the mesoporous PB nanoparticles. The functionalized nano-objects are able to deliver chloroquine using NIR light that in turn induces the phase-change of 1-tetradecanol to realize the combination of autophagy inhibition and photothermal therapy.

Remarkably, the PSM with drugs could also be achieved in non-hollow nanoparticles. Chen *et al.* described a multistep PSM procedure to enhance the DOX loading in PB nanoparticles.[191] Surface-free PB nanoparticles were first coated with oleylamine before a lipid-PEG conjugate was used to render the PB nanoparticles hydrophilic. The DOX, in its basic form, was then encapsulated into the hydrophobic lipid region of these PEGylated PB nanoparticles by taking advantage of hydrophobic interactions at the surface of the particles. The DOX loading is estimated at 9.2%. It was found that the drug release was enhanced at acidic pH, whereas *in vitro* studies indicate an enhanced killing of HeLa cells due to a synergistic effect between chemo and photothermal effect. Another

example of multistep surface functionalization was also reported by Lin *et al.*[197] Cubic PB nanoparticles of 55 nm obtained using citrate were firstly decorated with a layer of polydopamine before reaction with an amino PEG. Aiming to favour the nanoparticles accumulation in tumours while reducing side effects, folic acid was attached at the end of the PEG. In a last step, DOX could be loaded in the PEG shell *via* hydrogen and π–π interactions with a drug loading efficiency of 36%. The drug release could be triggered by both, pH and NIR stimuli. Similarly, citrate stabilized PB nanoparticles could be firstly coated with polydopamine and next reacted with human serum albumin that allows the DOX capture by hydrogen bonding based hydrophobic interactions with a loaded weight proportion estimated at 4.3%.[196] In another example, a red blood cell membrane was also associated with DOX and manganese-doped PB nanoparticles by a surface modification involving a co-extrusion method to increase the DOX loading capacity (estimated at 4.7%) and enhance the *in vivo* circulation time.[195] Remarkably, the system could catalyse the $H_2O_2$ conversion to generate oxygen, which relieves the hypoxia of tumours. This in turn disrupts the membrane and accelerates the DOX release.

To elucidate the adsorption mechanisms, a combined theoretical–experimental approach appears pivotal. Indeed, molecular simulations (Monte Carlo and DFT calculations) allow obtaining the saturation amount of guest molecules, which can be compared with experimental loading for further optimization processes (modification of solvent, *etc.*), as well as the interaction energy of these molecules with the framework. Besides, plausible configurations in the pores can also be extracted and adsorption sites can be elucidated. These simulations are validated by comparison between theoretical results and experimental data. Such a strategy has already been used for the drug adsorption in MOF materials.[244–247] It has for instance been possible to demonstrate the fact that the presence of solvent molecules prevents the entrance in some pores of MIL-100 due to the chemisorption of ethanol. Similar combined strategy starts now to be used in PB/PBA to understand the adsorption and co-adsorption of drug molecules in non-hollow nanoparticles without any stabilizer at their surface. Hence, using Monte Carlo simulations, it was demonstrated that the size of the DOX is clearly larger in comparison with the size of the pores generated by both, tetrahedral sites and hexacyanometallate single-vacancies.[221] Yet, it could not be excluded that PB/PBA most likely exhibit the presence of two adjacent vacancies leading to bi-lacunas with a greater accessible porosity, suitable to accommodate the DOX molecules, as described in Fig. 2. Nevertheless, the comparison between the experimental (7.6 wt%) and theoretical (5 wt% if only the amount adsorbed in the porosity is considered) capacities suggests that DOX is most likely simultaneously located within the porosity of the PB framework and at the surface. Once again, this highlights the fact that understanding the arrangement of lacunas in these cyano-bridged systems, as well as the clear picturing of the mode of interaction through both, experimental/theoretical approaches, are key parameters to enhance and control the loading of drugs, as well as other physico-chemical properties.

Although it will not be discussed here, the surface PSM could also be achieved by combining PB with other inorganic materials to design original core@shell architectures.[168] More generally, these results suggest that both, the nanoparticles' surface and internal porosity of the coordination network, could act together to improve the loading capacity of drugs in the aim to design multimodal theranostic agents.

### 5.2 Implementing luminescence in PB/PBA

Current technological demands in areas, such as nanothermometry,[248–250] sensors,[251,252] photonics,[253] and nanomedicine[254] concern the implementation of photoluminescence at the nanoscale. For instance, luminescence imaging is an affordable technique that benefits from a high temporal resolution and high sensitivity.[255] The combination of both properties within the same nano-object engenders several outcomes in both, fundamental and applied levels. Surprisingly, although efforts have been conducted to render nanosized PBA multifunctional, mainly for their possible use in the previously described applications, combination with luminescent probes remains relatively unexplored. PB belongs to the Robin and Day class II mixed-valence compound,[256] which implies semiconducting characteristics.[257] Thus, PB should exhibit photoluminescence inherent to its electronic band structure. Hence, the first example of weak photoluminescence of PB nanocubes in the UV-range was reported only in 2009.[258] A few years later a core@shell polypyrrole@PB nanoparticles obtained *via* mini-emulsion polymerization and exhibiting an emission around 600 nm was reported.[259] The differences in terms of emission wavelengths between the two systems have been ascribed to the change between the hollow and non-hollow PB nanoparticles. Incorporating polypyrrole inside the PB nanoshell induces a blue shift of the emission wavelength associated with an increase of the quantum yield.

In light of the recent development in the field of PB-based biomedical applications, it appears that luminescence imaging constitutes an efficient technique to fully develop the PB capabilities with the objective to easily monitor the nanoparticles uptake into the cells, follow their biodistribution and the efficiency of a photothermal/drug treatment. However, and with the aim to circumvent the weak luminescence of PB and tune the emission wavelengths, PSM represents a method of choice.

Firstly, the nanoparticle surface could be easily functionalized. For instance, Shokouhimehr *et al.* reported that either 5-(aminoacetamido)fluorescein[187] or Texas red cadeverine[149] dyes could be conjugated to citrate coated-nanoparticles through a chemical coupling to implement luminescence for *in vitro* fluorescence imaging. In 2014, Dumont *et al.* reported the PSM of surfactant-free $Mn^{2+}$-doped PB nanoparticles, whose surface was functionalized with the fluorescent avidin.[203] Noticeably, this latter allows the attachment of biotinylated ligands that target paediatric brain tumours. The observed green photoluminescence arises not from PB but

 

comes from the attached avidin moieties at the surface of the particles. *In vitro* and *ex vitro* fluorescence studies were used to study the organ biodistribution and in particularly the presence of nanoparticles in the brain. NIR fluorescence could also be implemented by functionalizing the surface serum albumin stabilized PB nanoparticles of 30 nm with the indocyanine green dye.[210] These functionalized nanoparticles act as a photothermal and photodynamic agents. An enhanced photothermal effect is therefore observed due to a synergistic effect between the two photothermal agents (PB and indocyanine green). The obtained nanoscaled system associates the dual magnetic resonance imaging features of PB with the NIR fluorescence imaging, as well as the photothermal and photodynamic therapies from both PB and indocyanine green.

The same indocyanine green dye could also be loaded into hollow PB nanoparticles modified by polyethyleneimine. Remarkably DOX could be subsequently loaded to provide a system exhibiting *in vivo* fluorescence imaging associated with light-induced chemo/photothermal/photodynamic therapies.[220]

This motivated to study in details the functionalization of PB/PBA particles with luminescent species using a PSM approach. Taking advantage of both, the surface and internal porosity approaches of the PSM, the incorporation/surface attachment of two fluorophores with different sizes, chemical functions and emission wavelengths has been considered (Fig. 8A and B).[167] On the one hand, 2-aminoanthracence (AA) exhibits a green emission, an amine function able to strongly interact with the active metal sites and a suitable size to be adsorbed into the pores of non-hollow nanoparticles generated by single hexacyanometallate vacancies (Fig. 1B). In contrast, the larger well-known rhodomine-B (RhB) dye could hardly access into the porosity of the coordination network, exhibits a red emission and show different possible interactions with the PB nanoparticles (electrostatic or covalent by the carboxylic moieties). The simple reaction between surfactant-free cubic PB nanoparticles of about 70 nm with the corresponding fluorophores in aqueous or ethanolic suspensions leads to the formation of PB@AA and PB@RhB. This simple strategy affords the formation of luminescent PB nanoparticles with emission wavelengths in the green or red regions (Fig. 8C), named PB@AA and PB@RhB, respectively. Remarkably, the photoluminescence could be observed in aqueous colloidal suspensions, in physiological conditions and in solid-state. The use of different experimental techniques in association with molecular modelling confirmed the adsorption mechanisms. As a result, AA is able to enter into the internal porosity of the PB framework (and may also possibly be located at the surface), while RhB is only attached at the nanoparticles surface. The estimated loading capacity of AA is of 7.6 wt% to be compared with the experimental one of 4.8 wt%. This suggests a competition with the solvent (EtOH) able to interact with the metal ions and/or diffusion issues during the adsorption of AA. The distribution of AA indicates that it is adsorbed in the pores generated by cyanometallate vacancies. Singularly, both functionalized systems (AA and RhB) do no exhibit a leakage of the fluorophores for several days indicating that such nanoprobes could be used for luminescence imaging. Hence, whereas the functionalized nanoparticles do not exhibit toxicity in the investigated concentration ranges, the cellular uptake and *in vitro* imaging of cancer cells confirmed that they could be efficiently used to follow the cell internationalization by luminescence imaging.

This approach was later extended to adsorption of fluorescent dyes eosin Y, rhodamine B and methylene blue in citrate-stabilized PB nanoparticles that have subsequently been decorated with PEG.[209]

In addition, most PBA also exhibits interesting magnetic properties, which could be easily tuned (magnetic transition temperature, coercive field, magnetization at saturation) depending on the choice of the metal ions.[260] Consequently, the association of magnetism and luminescence in multifunctional molecule-based nanosystems could be highly attractive to study the possible cross-effect between these properties, as well as for potential applications in sensors and electronics. The study of luminescent molecule-based magnets constitutes therefore an important topic.[261–266] However, combining these two functions appears challenging since most paramagnetic transition metal ions cause a quenching of the emission. In that sense, we recently demonstrated that both, ferromagnetic properties and luminescence could coexist in the functionalized nickel hexacyanochromate (NiCr) nanoparticles by using PSM.[223] This PBA analogue was selected because it does not exhibit strong absorption bands in the visible region that may cause a luminescence quenching. Moreover, it possesses a relatively high Curie temperature ($T_C$) characterizing the transition from paramagnetic to ferromagnetic state in its bulk form permitting to easily monitor the possible modifications in the magnetic behaviour. Thus, the PSM of nickel hexacyanochromate particles of 65 nm was performed by employing the AA dye, which is able to enter within the porosity of the cyano-bridged framework. This was confirmed both, experimentally and by Monte Carlo simulations. Investigations of the magnetic properties of the functionalized nanoparticles reveal that the characteristic ferromagnetic ordering related to the nickel hexacyanochromate PBA analogue with a $T_C$ at 65 K is preserved (Fig. 9A). In contrast, the photoluminescence is found

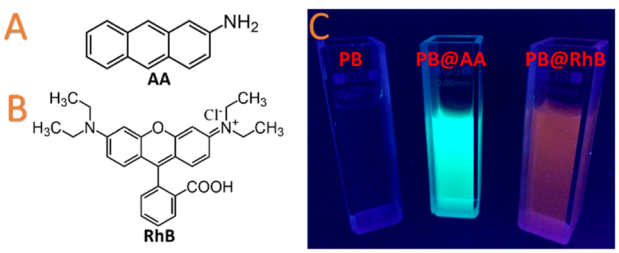


**Fig. 8** (A) Scheme of the 2-aminoanthracence (AA); (B) scheme of the rhodamine B (RhB); (C) photographs of aqueous suspensions of PB, PB@AA, and PB@RhB under excitation with an UV lamp at 365 nm showing their luminescence. Reprinted with permission from ref. 167. Copyright 2020 American Chemical Society.

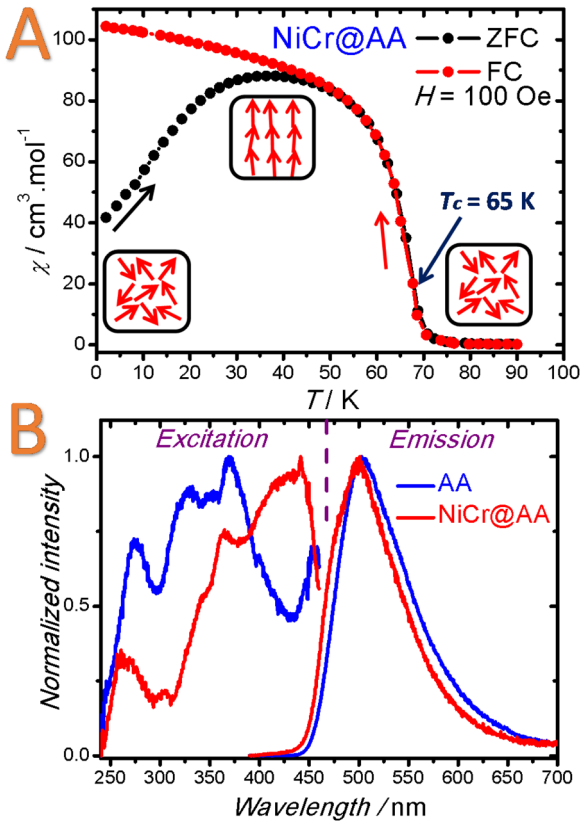


**Fig. 9** (A) Zero Field Cooled (ZFC)/Field Cooled (FC) curves performed for NiCr@AA with an applied magnetic field of 100 Oe and showing the Curie temperature ($T_C$) at 65 K; (B) room temperature excitation and emission spectra for NiCr@AA. Reproduced from ref. 223 with permission from the Royal Society of Chemistry.

to be slightly altered due to the modification of the AA environment caused by the interaction with the PBA framework (Fig. 9B). While the emission wavelength is found only slightly modified, the temperature dependence of both, the steady-state and emission lifetimes suggest differences in the non-radiative transition probabilities, which are found being exacerbated for the functionalized nanoparticles with respect to the free AA dye. Yet, the observation of both, a long-range magnetic ordering and luminescence constitutes a rare example of a luminescent molecule-based magnet.

## 6 Conclusions and perspectives

Owing to their high surface/volume ratio associated with their porous molecular structures, PB and PBA nanoparticles represent an original and promising platform to apply and develop PSM methods. On the one hand, the surface state of PB nanoparticles could be easily tuned by exploiting simple surface modification concepts to carefully tailor the physico-chemical and pharmaco-kinetic properties of the nano-objects.

On the other hand, the porous structure of PB/PBA could be exploited to modify or implement chemical or physical properties of nano-objects that could not be obtained by direct synthesis. The presence of cyanometallate vacancies generates simultaneously large pores and reactive metal sites. This allows adsorbing by PSM small functional guests (drugs, metal ions or dyes) that could interact at different levels with the cyano-bridged framework confirming its great flexibility. This opens exciting perspectives in various domains, such as catalysis, biomedical applications or separation. For instance, the chemical modification of the pores by ligand exchange may allow to greatly affecting the adsorption features, such as the hydrophobic/hydrophilic balance or the separation/sensing behaviour.[116] This could be achieved through a "coordination chemistry within the pores" approach by substituting or thermally removing the water molecules of the $[M(NC)_{6-x}(H_2O)_x]$ units and subsequent reactions with stronger ligands. One may therefore expect to chemically tune such cavities to specifically capture defined guests or drugs.

Moreover, additional interactions generated by the cyano-bridged coordination network might be further exploited. Although it has never been evidenced in the scope of nanoscaled PB/PBA, the π-character of cyano-ligands of the framework may be employed to promote π-interactions with appropriate guests. Such possibility has been largely exploited for the adsorption of hydrophobic guests in bulk PBA. For instance, it has been shown that the preferential interactions of cyclohexene with the PBA framework is explained by the π-character of CN bonds of the cobalt hexacyanocobaltate PBA.[117]

In addition, the presence of water molecules in the porosity might also mediate hydrogen bond interactions with the guest. Albeit theoretically possible, this mechanism has not been strongly evidenced to our knowledge in nanoscale PB/PBA systems. More generally, it appears that there is a lack of knowledge concerning the adsorption mechanisms in PB/PBA at the nanoscale. Among the upcoming challenges in the field, the in-depth understanding of the adsorption mechanisms, as well as the vacancies' arrangement in these non-stoichiometric nanomaterials appear fundamental. In this sense, the input of theoretical calculations to provide a full picture of the interaction appears critical to ultimately engineer enhanced systems.

Considering the recent development of PB nanoparticles in the biomedical field, the surface functionalization will appear as particularly decisive to assure the right biodistribution and organs or tissues targeting with the aim to take advantage of the theragnostic features of PB. In comparison with metal or metal oxides nanoparticles, the surface engineering of PB has not been deeply developed and an important effort are needed in order to provide a complete picture in this area.

Besides, new PSM routes need to be further explored. In this sense, the recent example of mechanochemical PSM in bulk PBA opens interesting perspectives since it would avoid solvent competition or chemical incompatibilities between the guest and the host frameworks.[267] Such methodology has to be fully implemented at the nanoscale. Furthermore, the possi-

 

bility to provide multistep PSM in the internal porosity of bulk PB/PBA has been rarely exploited. For comparison, a seven-step PSM methodology using peptidic coupling was used to introduce specific functional group in a MOF-74 that in turn proved to be an efficient catalyst.[268] Moreover, the PSM metal exchange, which is now widely employed in MOF chemistry,[25] has never been exploited to PB/PBA materials to the best of our knowledge. Post-substitution of transition metal ions constituting the PB/PBA frameworks will allow to introduce other metal or lanthanide ions to give additional functionalities.

Besides, we have demonstrated that additional properties could be implemented, such as luminescence in PB/PBA nanoparticles by simple guest adsorptions. It appears obvious that other features (chirality, conductivity, *etc*.) may be added by PSM by the careful choice of the functional guests. Furthermore and although it was not discussed in this review, the PSM could be easily extended to more complex PB architectures including core@shell heterostructures PBA@PBA′ or core@shell X@PBA or PBA@Y (X = Au, $Fe_3O_4$, Y = $SiO_2$),[10] expanding the number of possibilities.

The large adaptability of the cyano-bridged framework in terms of chemical compositions in concert with the PSM methodologies, both at the surface and in the internal porosity levels, will allow to accurately shape the chemical, physical and pharmaco-kinetic properties of these intriguing nanoscaled molecule-based materials.

## Conflicts of interest

There are no conflicts to declare.

## Acknowledgements

The authors thank the University of Montpellier, CNRS and PAC of ICGM. J. Lo. also acknowledges the support from the Institut Universitaire de France.

## Notes and references

1 A. Jaffe and J. R. Long, Ordered absences observed in porous framework materials, *Nature*, 2020, **578**, 222–223.
2 S. P. Moulik, G. C. De, A. K. Panda, B. B. Bhowmik and A. R. Das, Dispersed Molecular Aggregates. 1. Synthesis and Characterization of Nanoparticles of $Cu_2[Fe(CN)_6]$ in $H_2O$/AOT/n-Heptane Water-in-Oil Microemulsion Media, *Langmuir*, 1999, **15**, 8361–8367.
3 S. Vaucher, M. Li and S. Mann, Synthesis of Prussian Blue Nanoparticles and Nanocrystal Superlattices in Reverse Microemulsions, *Angew. Chem., Int. Ed.*, 2000, **39**, 1793–1796.
4 Y. Guari and J. Larionova, *Prussian Blue-Type Nanoparticles and Nanocomposites: Synthesis, Devices, and Applications*, CRC Press, 2019.
5 X. Wang and L. Cheng, Multifunctional Prussian blue-based nanomaterials: Preparation, modification, and theranostic applications, *Coord. Chem. Rev.*, 2020, **419**, 213393.
6 E. Dujardin and S. Mann, Morphosynthesis of Molecular Magnetic Materials, *Adv. Mater.*, 2004, **16**, 1125–1129.
7 J. Larionova, Y. Guari, C. Sangregorio and C. Guerin, Cyano-bridged coordination polymer nanoparticles, *New J. Chem.*, 2009, **33**, 1177–1190.
8 L. Catala, F. Volatron, D. Brinzei and T. Mallah, Functional Coordination Nanoparticles, *Inorg. Chem.*, 2009, **48**, 3360–3370.
9 J. Long, Y. Guari, C. Guerin and J. Larionova, Prussian blue type nanoparticles for biomedical applications, *Dalton Trans.*, 2016, **45**, 17581–17587.
10 L. Catala and T. Mallah, Nanoparticles of Prussian blue analogs and related coordination polymers: From information storage to biomedical applications, *Coord. Chem. Rev.*, 2017, **346**, 32–61.
11 Z. Qin, Y. Li and N. Gu, Progress in Applications of Prussian Blue Nanoparticles in Biomedicine, *Adv. Healthcare Mater.*, 2018, **7**, 1800347.
12 M. Gautam, K. Poudel, C. S. Yong and J. O. Kim, Prussian blue nanoparticles: Synthesis, surface modification, and application in cancer treatment, *Int. J. Pharm.*, 2018, **549**, 31–49.
13 N. Sanvicens and M. P. Marco, Multifunctional nanoparticles – properties and prospects for their use in human medicine, *Trends Biotechnol.*, 2008, **26**, 425–433.
14 G. Bao, S. Mitragotri and S. Tong, Multifunctional Nanoparticles for Drug Delivery and Molecular Imaging, *Annu. Rev. Biomed. Eng.*, 2013, **15**, 253–282.
15 S. T. Selvan, T. T. Y. Tan, D. K. Yi and N. R. Jana, Functional and Multifunctional Nanoparticles for Bioimaging and Biosensing, *Langmuir*, 2010, **26**, 11631–11641.
16 P. J. J. Alvarez, C. K. Chan, M. Elimelech, N. J. Halas and D. Villagrán, Emerging opportunities for nanotechnology to enhance water security, *Nat. Nanotechnol.*, 2018, **13**, 634–641.
17 D. Gontero, M. Lessard-Viger, D. Brouard, A. G. Bracamonte, D. Boudreau and A. V. Veglia, Smart multifunctional nanoparticles design as sensors and drug delivery systems based on supramolecular chemistry, *Microchem. J.*, 2017, **130**, 316–328.
18 H. Tokoro and S.-i. Ohkoshi, Novel magnetic functionalities of Prussian blue analogs, *Dalton Trans.*, 2011, **40**, 6825–6833.
19 R. A. Sperling and W. J. Parak, Surface modification, functionalization and bioconjugation of colloidal inorganic nanoparticles, *Philos. Trans. R. Soc., A*, 2010, **368**, 1333–1383.
20 S. Kango, S. Kalia, A. Celli, J. Njuguna, Y. Habibi and R. Kumar, Surface modification of inorganic nanoparticles for development of organic–inorganic nanocomposites—A review, *Prog. Polym. Sci.*, 2013, **38**, 1232–1261.

21 J. L. Stein, E. A. Mader and B. M. Cossairt, Luminescent InP Quantum Dots with Tunable Emission by Post-Synthetic Modification with Lewis Acids, *J. Phys. Chem. Lett.*, 2016, **7**, 1315–1320.
22 D. Brühwiler, Postsynthetic functionalization of mesoporous silica, *Nanoscale*, 2010, **2**, 887–892.
23 M. Laghaei, M. Sadeghi, B. Ghalei and M. Dinari, The effect of various types of post-synthetic modifications on the structure and properties of MCM-41 mesoporous silica, *Prog. Org. Coat.*, 2016, **90**, 163–170.
24 K. K. Tanabe and S. M. Cohen, Postsynthetic modification of metal–organic frameworks—a progress report, *Chem. Soc. Rev.*, 2011, **40**, 498–519.
25 Z. Yin, S. Wan, J. Yang, M. Kurmoo and M.-H. Zeng, Recent advances in post-synthetic modification of metal–organic frameworks: New types and tandem reactions, *Coord. Chem. Rev.*, 2019, **378**, 500–512.
26 Z. Wang and S. M. Cohen, Postsynthetic modification of metal–organic frameworks, *Chem. Soc. Rev.*, 2009, **38**, 1315–1329.
27 Z. P. Xu, Q. H. Zeng, G. Q. Lu and A. B. Yu, Inorganic nanoparticles as carriers for efficient cellular delivery, *Chem. Eng. Sci.*, 2006, **61**, 1027–1040.
28 W. Wu, Q. He and C. Jiang, Magnetic iron oxide nanoparticles: synthesis and surface functionalization strategies, *Nanoscale Res. Lett.*, 2008, **3**, 397.
29 N. Erathodiyil and J. Y. Ying, Functionalization of Inorganic Nanoparticles for Bioimaging Applications, *Acc. Chem. Res.*, 2011, **44**, 925–935.
30 J. Conde, J. T. Dias, V. Grazú, M. Moros, P. V. Baptista and J. M. de la Fuente, Revisiting 30 years of biofunctionalization and surface chemistry of inorganic nanoparticles for nanomedicine, *Front. Chem.*, 2014, **2**, 48.
31 A. Liberman, N. Mendez, W. C. Trogler and A. C. Kummel, Synthesis and surface functionalization of silica nanoparticles for nanomedicine, *Surf. Sci. Rep.*, 2014, **69**, 132–158.
32 T. T. H. Thi, T. N. Q. Nguyen, D. T. Hoang and D. H. Nguyen, Functionalized mesoporous silica nanoparticles and biomedical applications, *Mater. Sci. Eng., C*, 2019, **99**, 631–656.
33 J. Kecht, A. Schlossbauer and T. Bein, Selective functionalization of the outer and inner surfaces in mesoporous silica nanoparticles, *Chem. Mater.*, 2008, **20**, 7207–7214.
34 S. Wang, C. M. McGuirk, A. d'Aquino, J. A. Mason and C. A. Mirkin, Metal–Organic Framework Nanoparticles, *Adv. Mater.*, 2018, **30**, 1800202.
35 Q. Wang and D. Astruc, State of the Art and Prospects in Metal–Organic Framework (MOF)-Based and MOF-Derived Nanocatalysis, *Chem. Rev.*, 2020, **120**, 1438–1511.
36 E. Ploetz, H. Engelke, U. Lächelt and S. Wuttke, The Chemistry of Reticular Framework Nanoparticles: MOF, ZIF, and COF Materials, *Adv. Funct. Mater.*, 2020, **30**, 1909062.
37 Y. Bai, Y. Dou, L.-H. Xie, W. Rutledge, J.-R. Li and H.-C. Zhou, Zr-based metal–organic frameworks: design, synthesis, structure, and applications, *Chem. Soc. Rev.*, 2016, **45**, 2327–2367.
38 T.-Y. Liu, X.-L. Qu and B. Yan, A sensitive metal–organic framework nanosensor with cation-introduced chirality for enantioselective recognition and determination of quinine and quinidine in human urine, *J. Mater. Chem. C*, 2020, **8**, 14579–14586.
39 J. Meng, X. Liu, C. Niu, Q. Pang, J. Li, F. Liu, Z. Liu and L. Mai, Advances in metal–organic framework coatings: versatile synthesis and broad applications, *Chem. Soc. Rev.*, 2020, **49**, 3142–3186.
40 Z. Ji, H. Z. Wang, S. Canossa, S. Wuttke and O. M. Yaghi, Pore Chemistry of Metal-Organic Frameworks, *Adv. Funct. Mater.*, 2020, **30**, 2000238.
41 Y. Kim and S. Huh, Pore engineering of metal–organic frameworks: introduction of chemically accessible Lewis basic sites inside MOF channels, *CrystEngComm*, 2016, **18**, 3524–3550.
42 F. Sun, Z. Yin, Q.-Q. Wang, D. Sun, M.-H. Zeng and M. Kurmoo, Tandem Postsynthetic Modification of a Metal–Organic Framework by Thermal Elimination and Subsequent Bromination: Effects on Absorption Properties and Photoluminescence, *Angew. Chem., Int. Ed.*, 2013, **52**, 4538–4543.
43 M. Zhang, T. Yang, Z. Wang, X.-F. Ma, Y. Zhang, S. M. Greer, S. A. Stoian, Z.-W. Ouyang, H. Nojiri, M. Kurmoo and M.-H. Zeng, Chemical reaction within a compact non-porous crystal containing molecular clusters without the loss of crystallinity, *Chem. Sci.*, 2017, **8**, 5356–5361.
44 Z. Wang and S. M. Cohen, Postsynthetic Covalent Modification of a Neutral Metal–Organic Framework, *J. Am. Chem. Soc.*, 2007, **129**, 12368–12369.
45 M. Dincă and J. R. Long, High-Enthalpy Hydrogen Adsorption in Cation-Exchanged Variants of the Microporous Metal–Organic Framework $Mn_3[(Mn_4Cl)_3(BTT)_8(CH_3OH)_{10}]_2$, *J. Am. Chem. Soc.*, 2007, **129**, 11172–11176.
46 M. Banerjee, S. Das, M. Yoon, H. J. Choi, M. H. Hyun, S. M. Park, G. Seo and K. Kim, Postsynthetic Modification Switches an Achiral Framework to Catalytically Active Homochiral Metal–Organic Porous Materials, *J. Am. Chem. Soc.*, 2009, **131**, 7524–7525.
47 S. Cheng, Y. Wu, J. Jin, J. Liu, D. Wu, G. Yang and Y.-Y. Wang, New multifunctional 3D porous metal–organic framework with selective gas adsorption, efficient chemical fixation of $CO_2$ and dye adsorption, *Dalton Trans.*, 2019, **48**, 7612–7618.
48 J. Rocha, L. D. Carlos, F. A. A. Paz and D. Ananias, Luminescent multifunctional lanthanides-based metal–organic frameworks, *Chem. Soc. Rev.*, 2011, **40**, 926–940.
49 Y. Cui, Y. Yue, G. Qian and B. Chen, Luminescent Functional Metal–Organic Frameworks, *Chem. Rev.*, 2012, **112**, 1126–1162.
50 P. Railey, Y. Song, T. Liu and Y. Li, Metal organic frameworks with immobilized nanoparticles: Synthesis and

 

applications in photocatalytic hydrogen generation and energy storage, *Mater. Res. Bull.*, 2017, **96**, 385–394.
51 A. Corma, H. García and F. X. Llabrés i Xamena, Engineering Metal Organic Frameworks for Heterogeneous Catalysis, *Chem. Rev.*, 2010, **110**, 4606–4655.
52 P. Horcajada, R. Gref, T. Baati, P. K. Allan, G. Maurin, P. Couvreur, G. Férey, R. E. Morris and C. Serre, Metal–Organic Frameworks in Biomedicine, *Chem. Rev.*, 2012, **112**, 1232–1268.
53 Q.-L. Zhu and Q. Xu, Metal–organic framework composites, *Chem. Soc. Rev.*, 2014, **43**, 5468–5512.
54 L. Chen, R. Luque and Y. Li, Controllable design of tunable nanostructures inside metal–organic frameworks, *Chem. Soc. Rev.*, 2017, **46**, 4614–4630.
55 Y. Zhang, S. Yuan, G. Day, X. Wang, X. Yang and H.-C. Zhou, Luminescent sensors based on metal-organic frameworks, *Coord. Chem. Rev.*, 2018, **354**, 28–45.
56 L. Wang, M. Zheng and Z. Xie, Nanoscale metal–organic frameworks for drug delivery: a conventional platform with new promise, *J. Mater. Chem. B*, 2018, **6**, 707–717.
57 J. Canivet, A. Fateeva, Y. Guo, B. Coasne and D. Farrusseng, Water adsorption in MOFs: fundamentals and applications, *Chem. Soc. Rev.*, 2014, **43**, 5594–5617.
58 J. Duan, W. Jin and S. Kitagawa, Water-resistant porous coordination polymers for gas separation, *Coord. Chem. Rev.*, 2017, **332**, 48–74.
59 A. J. Rieth, A. M. Wright and M. Dincă, Kinetic stability of metal–organic frameworks for corrosive and coordinating gas capture, *Nat. Rev. Mater.*, 2019, **4**, 708–725.
60 H. N. Rubin and M. M. Reynolds, Functionalization of Metal–Organic Frameworks To Achieve Controllable Wettability, *Inorg. Chem.*, 2017, **56**, 5266–5274.
61 S. M. F. Vilela, P. Salcedo-Abraira, A. Gómez-Peña, P. Trens, A. Várez, F. Salles and P. Horcajada, Proton Conductive Zr-Phosphonate UPG-1—Aminoacid Insertion as Proton Carrier Stabilizer, *Molecules*, 2020, **25**, 3519.
62 H. W. B. Teo, A. Chakraborty and S. Kayal, Post synthetic modification of MIL-101(Cr) for S-shaped isotherms and fast kinetics with water adsorption, *Appl. Therm. Eng.*, 2017, **120**, 453–462.
63 S. Rojas, T. Devic and P. Horcajada, Metal organic frameworks based on bioactive components, *J. Mater. Chem. B*, 2017, **5**, 2560–2573.
64 T. Gadzikwa, G. Lu, C. L. Stern, S. R. Wilson, J. T. Hupp and S. T. Nguyen, Covalent surface modification of a metal–organic framework: selective surface engineering via CuI-catalyzed Huisgen cycloaddition, *Chem. Commun.*, 2008, 5493–5495.
65 F. Sun, Z. Yin, Q.-Q. Wang, D. Sun, M.-H. Zeng and M. Kurmoo, Tandem Postsynthetic Modification of a Metal–Organic Framework by Thermal Elimination and Subsequent Bromination: Effects on Absorption Properties and Photoluminescence, *Angew. Chem., Int. Ed.*, 2013, **52**, 4538–4543.
66 S. Kaskel, *The Chemistry of Metal-Organic Frameworks, 2 Volume Set: Synthesis, Characterization, and Applications*, John Wiley & Sons, 2016.
67 C. V. McGuire and R. S. Forgan, The surface chemistry of metal–organic frameworks, *Chem. Commun.*, 2015, **51**, 5199–5217.
68 R. S. Forgan, The surface chemistry of metal–organic frameworks and their applications, *Dalton Trans.*, 2019, **48**, 9037–9042.
69 W. J. Rieter, K. M. L. Taylor, H. An, W. Lin and W. Lin, Nanoscale Metal–Organic Frameworks as Potential Multimodal Contrast Enhancing Agents, *J. Am. Chem. Soc.*, 2006, **128**, 9024–9025.
70 P. Horcajada, T. Chalati, C. Serre, B. Gillet, C. Sebrie, T. Baati, J. F. Eubank, D. Heurtaux, P. Clayette, C. Kreuz, J.-S. Chang, Y. K. Hwang, V. Marsaud, P.-N. Bories, L. Cynober, S. Gil, G. Férey, P. Couvreur and R. Gref, Porous metal–organic-framework nanoscale carriers as a potential platform for drug delivery and imaging, *Nat. Mater.*, 2010, **9**, 172–178.
71 R. C. Huxford, K. E. deKrafft, W. S. Boyle, D. Liu and W. Lin, Lipid-coated nanoscale coordination polymers for targeted delivery of antifolates to cancer cells, *Chem. Sci.*, 2012, **3**, 198–204.
72 J. Chun, S. Kang, N. Park, E. J. Park, X. Jin, K.-D. Kim, H. O. Seo, S. M. Lee, H. J. Kim, W. H. Kwon, Y.-K. Park, J. M. Kim, Y. D. Kim and S. U. Son, Metal–Organic Framework@Microporous Organic Network: Hydrophobic Adsorbents with a Crystalline Inner Porosity, *J. Am. Chem. Soc.*, 2014, **136**, 6786–6789.
73 M. Kondo, S. Furukawa, K. Hirai and S. Kitagawa, Coordinatively Immobilized Monolayers on Porous Coordination Polymer Crystals, *Angew. Chem., Int. Ed.*, 2010, **49**, 5327–5330.
74 N. Yanai, M. Sindoro, J. Yan and S. Granick, Electric Field-Induced Assembly of Monodisperse Polyhedral Metal–Organic Framework Crystals, *J. Am. Chem. Soc.*, 2013, **135**, 34–37.
75 X. Liu, Y. Li, Y. Ban, Y. Peng, H. Jin, H. Bux, L. Xu, J. Caro and W. Yang, Improvement of hydrothermal stability of zeolitic imidazolate frameworks, *Chem. Commun.*, 2013, **49**, 9140–9142.
76 M. D. Rowe, D. H. Thamm, S. L. Kraft and S. G. Boyes, Polymer-Modified Gadolinium Metal-Organic Framework Nanoparticles Used as Multifunctional Nanomedicines for the Targeted Imaging and Treatment of Cancer, *Biomacromolecules*, 2009, **10**, 983–993.
77 H. G. T. Nguyen, M. H. Weston, O. K. Farha, J. T. Hupp and S. T. Nguyen, A catalytically active vanadyl(catecholate)-decorated metal organic framework via post-synthesis modifications, *CrystEngComm*, 2012, **14**, 4115–4118.
78 M.-X. Wu and Y.-W. Yang, Metal–Organic Framework (MOF)-Based Drug/Cargo Delivery and Cancer Therapy, *Adv. Mater.*, 2017, **29**, 1606134.
79 R. Röder, T. Preiß, P. Hirschle, B. Steinborn, A. Zimpel, M. Höhn, J. O. Rädler, T. Bein, E. Wagner, S. Wuttke and

U. Lächelt, Multifunctional Nanoparticles by Coordinative Self-Assembly of His-Tagged Units with Metal–Organic Frameworks, *J. Am. Chem. Soc.*, 2017, **139**, 2359–2368.

80 G. Fan, C. M. Dundas, C. Zhang, N. A. Lynd and B. K. Keitz, Sequence-Dependent Peptide Surface Functionalization of Metal–Organic Frameworks, *ACS Appl. Mater. Interfaces*, 2018, **10**, 18601–18609.

81 S. Wang, C. M. McGuirk, M. B. Ross, S. Wang, P. Chen, H. Xing, Y. Liu and C. A. Mirkin, General and Direct Method for Preparing Oligonucleotide-Functionalized Metal–Organic Framework Nanoparticles, *J. Am. Chem. Soc.*, 2017, **139**, 9827–9830.

82 S. Wang, Y. Chen, S. Wang, P. Li, C. A. Mirkin and O. K. Farha, DNA-Functionalized Metal–Organic Framework Nanoparticles for Intracellular Delivery of Proteins, *J. Am. Chem. Soc.*, 2019, **141**, 2215–2219.

83 S. Jung, Y. Kim, S.-J. Kim, T.-H. Kwon, S. Huh and S. Park, Bio-functionalization of metal–organic frameworks by covalent protein conjugation, *Chem. Commun.*, 2011, **47**, 2904–2906.

84 P.-Z. Li, X.-J. Wang and Y. Zhao, Click chemistry as a versatile reaction for construction and modification of metal-organic frameworks, *Coord. Chem. Rev.*, 2019, **380**, 484–518.

85 C. R. Quijia, C. Lima, C. Silva, R. C. Alves, R. Frem and M. Chorilli, Application of MIL-100(Fe) in drug delivery and biomedicine, *J. Drug Delivery Sci. Technol.*, 2021, **61**, 102217.

86 A. G. Márquez, T. Hidalgo, H. Lana, D. Cunha, M. J. Blanco-Prieto, C. Álvarez-Lorenzo, C. Boissière, C. Sánchez, C. Serre and P. Horcajada, Biocompatible polymer–metal–organic framework composite patches for cutaneous administration of cosmetic molecules, *J. Mater. Chem. B*, 2016, **4**, 7031–7040.

87 S. D. Taherzade, S. Rojas, J. Soleimannejad and P. Horcajada, Combined Cutaneous Therapy Using Biocompatible Metal-Organic Frameworks, *Nanomaterials*, 2020, **10**, 2296.

88 A. Kraft, On the discovery and history of Prussian blue, *Bull. Hist. Chem.*, 2008, **33**, 61–67.

89 B. Nayebi, K. P. Niavol, B. Nayebi, S. Y. Kim, K. T. Nam, H. W. Jang, R. S. Varma and M. Shokouhimehr, Prussian blue-based nanostructured materials: Catalytic applications for environmental remediation and energy conversion, *Mol. Catal.*, 2021, **514**, 111835.

90 J. Qian, C. Wu, Y. Cao, Z. Ma, Y. Huang, X. Ai and H. Yang, Prussian Blue Cathode Materials for Sodium-Ion Batteries and Other Ion Batteries, *Adv. Energy Mater.*, 2018, **8**, 1702619.

91 K. Hurlbutt, S. Wheeler, I. Capone and M. Pasta, Prussian Blue Analogs as Battery Materials, *Joule*, 2018, **2**, 1950–1960.

92 M. Okubo, J. Long, D. R. Talham and R. Lescouëzec, Solid-state electrochemistry of metal cyanides, *C. R. Chim.*, 2019, **22**, 483–489.

93 J. Peng, W. Zhang, Q. Liu, J. Wang, S. Chou, H. Liu and S. Dou, Prussian Blue Analogues for Sodium-Ion Batteries: Past, Present, and Future, *Adv. Mater.*, 2022, **34**, 2108384.

94 A. Takahashi, H. Tanaka, K. Minami, K. Noda, M. Ishizaki, M. Kurihara, H. Ogawa and T. Kawamoto, Unveiling Cs-adsorption mechanism of Prussian blue analogs: $Cs^+$-percolation via vacancies to complete dehydrated state, *RSC Adv.*, 2018, **8**, 34808–34816.

95 S. S. Kaye and J. R. Long, Hydrogen Storage in the Dehydrated Prussian Blue Analogues $M_3[Co(CN)_6]_2$ (M = Mn, Fe, Co, Ni, Cu, Zn), *J. Am. Chem. Soc.*, 2005, **127**, 6506–6507.

96 B. Zamora, J. Roque, J. Balmaseda and E. Reguera, Methane Storage in Prussian Blue Analogues and Related Porous Solids: Nature of the Involved Adsorption Forces, *Z. Anorg. Allg. Chem.*, 2010, **636**, 2574–2578.

97 J. Roque, E. Reguera, J. Balmaseda, J. Rodríguez-Hernández, L. Reguera and L. F. del Castillo, Porous hexacyanocobaltates(III): Role of the metal on the framework properties, *Microporous Mesoporous Mater.*, 2007, **103**, 57–71.

98 J. Long, Y. Guari, C. Guérin and J. Larionova, Prussian blue type nanoparticles for biomedical applications, *Dalton Trans.*, 2016, **45**, 17581–17587.

99 H.-W. Lee, R. Y. Wang, M. Pasta, S. Woo Lee, N. Liu and Y. Cui, Manganese hexacyanomanganate open framework as a high-capacity positive electrode material for sodium-ion batteries, *Nat. Commun.*, 2014, **5**, 5280.

100 Y. Xu, J. Wan, L. Huang, M. Ou, C. Fan, P. Wei, J. Peng, Y. Liu, Y. Qiu, X. Sun, C. Fang, Q. Li, J. Han, Y. Huang, J. A. Alonso and Y. Zhao, Structure Distortion Induced Monoclinic Nickel Hexacyanoferrate as High-Performance Cathode for Na-Ion Batteries, *Adv. Energy Mater.*, 2019, **9**, 1803158.

101 W. Kosaka, T. Ishihara, H. Yashiro, Y. Taniguchi, K. Hashimoto and S.-i. Ohkoshi, Synthesis of Ferromagnetic CsCuCr Prussian Blue Analogue with a Tetragonal Structure, *Chem. Lett.*, 2005, **34**, 1278–1279.

102 G. Azzolina, R. Bertoni, C. Ecolivet, H. Tokoro, S.-i. Ohkoshi and E. Collet, Landau theory for non-symmetry-breaking electronic instability coupled to symmetry-breaking order parameter applied to Prussian blue analog, *Phys. Rev. B*, 2020, **102**, 134104.

103 W. Wang, Y. Gang, Z. Hu, Z. Yan, W. Li, Y. Li, Q.-F. Gu, Z. Wang, S.-L. Chou, H.-K. Liu and S.-X. Dou, Reversible structural evolution of sodium-rich rhombohedral Prussian blue for sodium-ion batteries, *Nat. Commun.*, 2020, **11**, 980.

104 Y. You, X.-L. Wu, Y.-X. Yin and Y.-G. Guo, High-quality Prussian blue crystals as superior cathode materials for room-temperature sodium-ion batteries, *Energy Environ. Sci.*, 2014, **7**, 1643–1647.

105 G. Du and H. Pang, Recent advancements in Prussian blue analogues: Preparation and application in batteries, *Energy Storage Mater.*, 2021, **36**, 387–408.

106 S. S. Kaye and J. R. Long, The role of vacancies in the hydrogen storage properties of Prussian blue analogues, *Catal. Today*, 2007, **120**, 311–316.

107 A. Simonov, T. De Baerdemaeker, H. L. B. Boström, M. L. Ríos Gómez, H. J. Gray, D. Chernyshov, A. Bosak,

 

H.-B. Bürgi and A. L. Goodwin, Hidden diversity of vacancy networks in Prussian blue analogues, *Nature*, 2020, **578**, 256–260.

108 A. Flambard, F. H. Köhler and R. Lescouëzec, Revisiting Prussian Blue Analogues with Solid-State MAS NMR Spectroscopy: Spin Density and Local Structure in $[Cd_3\{Fe(CN)_6\}_2]\cdot 15H_2O$, *Angew. Chem., Int. Ed.*, 2009, **48**, 1673–1676.

109 S. Ganguli and M. Bhattacharya, Studies of different hydrated forms of Prussian Blue, *J. Chem. Soc., Faraday Trans. 1*, 1983, **79**, 1513–1522.

110 F. Grandjean, L. Samain and G. J. Long, Characterization and utilization of Prussian blue and its pigments, *Dalton Trans.*, 2016, **45**, 18018–18044.

111 P. Franz, C. Ambrus, A. Hauser, D. Chernyshov, M. Hostettler, J. Hauser, L. Keller, K. Krämer, H. Stoeckli-Evans, P. Pattison, H.-B. Bürgi and S. Decurtins, Crystalline, Mixed-Valence Manganese Analogue of Prussian Blue: Magnetic, Spectroscopic, X-ray and Neutron Diffraction Studies, *J. Am. Chem. Soc.*, 2004, **126**, 16472–16477.

112 S. Liu and K. C. Smith, Intercalated Cation Disorder in Prussian Blue Analogues: First-Principles and Grand Canonical Analyses, *J. Phys. Chem. C*, 2019, **123**, 10191–10204.

113 M. J. Cliffe, E. N. Keyzer, A. D. Bond, M. A. Astle and C. P. Grey, The structures of ordered defects in thiocyanate analogues of Prussian Blue, *Chem. Sci.*, 2020, **11**, 4430–4438.

114 M. P. Shores, L. G. Beauvais and J. R. Long, Cluster-Expanded Prussian Blue Analogues, *J. Am. Chem. Soc.*, 1999, **121**, 775–779.

115 S. S. Kaye, H. J. Choi and J. R. Long, Generation and $O_2$ Adsorption Studies of the Microporous Magnets CsNi[Cr(CN)$_6$] ($T_C$ = 75 K) and $Cr_3[Cr(CN)_6]_2\cdot 6H_2O$ ($T_N$ = 219 K), *J. Am. Chem. Soc.*, 2008, **130**, 16921–16925.

116 L. Boudjema, J. Long, F. Salles, J. Larionova, Y. Guari and P. Trens, A Switch in the Hydrophobic/Hydrophilic Gas-Adsorption Character of Prussian Blue Analogues: An Affinity Control for Smart Gas Sorption, *Chem. – Eur. J.*, 2019, **25**, 479–484.

117 L. Boudjema, J. Long, H. Petitjean, J. Larionova, Y. Guari, P. Trens and F. Salles, Adsorption of Volatile Organic Compounds by ZIF-8, Cu-BTC and a Prussian blue analogue: A comparative study, *Inorg. Chim. Acta*, 2019, **501**, 119316.

118 L. Boudjema, E. Mamontova, J. Long, J. Larionova, Y. Guari and P. Trens, Prussian Blue Analogues for the Separation of Hydrocarbons in Humid Conditions, *Inorg. Chem.*, 2017, **56**, 7598–7601.

119 A. Takahashi, H. Tanaka, D. Parajuli, T. Nakamura, K. Minami, Y. Sugiyama, Y. Hakuta, S.-i. Ohkoshi and T. Kawamoto, Historical Pigment Exhibiting Ammonia Gas Capture beyond Standard Adsorbents with Adsorption Sites of Two Kinds, *J. Am. Chem. Soc.*, 2016, **138**, 6376–6379.

120 J. Estelrich and M. A. Busquets, Prussian Blue: A Safe Pigment with Zeolitic-Like Activity, *Int. J. Mol. Sci.*, 2021, **22**(2), 780.

121 T. Kameda, H. Kikuchi, F. Kitagawa, S. Kumagai, Y. Saito, M. Kondo, Y. Jimbo and T. Yoshioka, Ammonia adsorption by L-type zeolite and Prussian blue from aqueous and culture solutions, *Colloids Surf., A*, 2021, **622**, 126595.

122 F. Salles, H. Jobic, T. Devic, V. Guillerm, C. Serre, M. M. Koza, G. Ferey and G. Maurin, Diffusion of Binary $CO_2/CH_4$ Mixtures in the MIL-47(V) and MIL-53(Cr) Metal–Organic Framework Type Solids: A Combination of Neutron Scattering Measurements and Molecular Dynamics Simulations, *J. Phys. Chem. C*, 2013, **117**, 11275–11284.

123 F. Salles, G. Maurin, C. Serre, P. L. Llewellyn, C. Knöfel, H. J. Choi, Y. Filinchuk, L. Oliviero, A. Vimont, J. R. Long and G. Férey, Multistep $N_2$ Breathing in the Metal–Organic Framework Co(1,4-benzenedipyrazolate), *J. Am. Chem. Soc.*, 2010, **132**, 13782–13788.

124 M. Pyrasch, A. Toutianoush, W. Jin, J. Schnepf and B. Tieke, Self-assembled Films of Prussian Blue and Analogues: Optical and Electrochemical Properties and Application as Ion-Sieving Membranes, *Chem. Mater.*, 2003, **15**, 245–254.

125 L. Ma, H. Cui, S. Chen, X. Li, B. Dong and C. Zhi, Accommodating diverse ions in Prussian blue analogs frameworks for rechargeable batteries: The electrochemical redox reactions, *Nano Energy*, 2021, **81**, 105632.

126 A. K. Vipin, B. Fugetsu, I. Sakata, A. Isogai, M. Endo, M. Li and M. S. Dresselhaus, Cellulose nanofiber backboned Prussian blue nanoparticles as powerful adsorbents for the selective elimination of radioactive cesium, *Sci. Rep.*, 2016, **6**, 37009.

127 W. Stevens, C. van Peteghem, A. Heyndrickx and F. Barbier, Eleven cases of thallium intoxication treated with Prussian blue, *Int. J. Clin. Pharmacol., Ther. Toxicol.*, 1974, **10**, 1–22.

128 K. Madshus, A. Strömme, F. Bohne and V. Nigrović, Diminution of Radiocaesium Body-burden in Dogs and Human Beings by Prussian Blue, *Int. J. Radiat. Biol. Relat. Stud. Phys., Chem. Med.*, 1966, **10**, 519–520.

129 H. Heydlauf, Ferric-cyanoferrate(II): An effective antidote in thallium poisoning, *Eur. J. Pharmacol.*, 1969, **6**, 340–344.

130 A. A. Vrij, H. M. H. G. Cremers and F. A. Th. Lustermans, Successful recovery of a patient with thallium poisoning, *Neth. J. Med.*, 1995, **47**, 121–126.

131 D. F. Thompson and C. O. Church, Prussian blue for treatment of radiocesium poisoning, *Pharmacotherapy*, 2001, **21**, 1364–1367.

132 D. F. Thompson and E. D. Callen, Soluble or insoluble Prussian blue for radiocesium and thallium poisoning?, *Ann. Pharmacother.*, 2004, **38**, 1509–1514.

133 P. J. Faustino, Y. Yang, J. J. Progar, C. R. Brownell, N. Sadrieh, J. C. May, E. Leutzinger, D. A. Place, E. P. Duffy, F. Houn, S. A. Loewke, V. J. Mecozzi,

C. D. Ellison, M. A. Khan, A. S. Hussain and R. C. Lyon, Quantitative determination of cesium binding to ferric hexacyanoferrate: Prussian blue, *J. Pharm. Biomed. Anal.*, 2008, **47**, 114–125.

134 M. Ishizaki, S. Akiba, A. Ohtani, Y. Hoshi, K. Ono, M. Matsuba, T. Togashi, K. Kananizuka, M. Sakamoto, A. Takahashi, T. Kawamoto, H. Tanaka, M. Watanabe, M. Arisaka, T. Nankawa and M. Kurihara, Proton-exchange mechanism of specific $Cs^+$ adsorption via lattice defect sites of Prussian blue filled with coordination and crystallization water molecules, *Dalton Trans.*, 2013, **42**, 16049–16055.

135 X. Wu, Y. Qi, J. J. Hong, Z. Li, A. S. Hernandez and X. Ji, Rocking-Chair Ammonium-Ion Battery: A Highly Reversible Aqueous Energy Storage System, *Angew. Chem., Int. Ed.*, 2017, **56**, 13026–13030.

136 S. Vaucher, J. Fielden, M. Li, E. Dujardin and S. Mann, Molecule-Based Magnetic Nanoparticles: Synthesis of Cobalt Hexacyanoferrate, Cobalt Pentacyanonitrosylferrate, and Chromium Hexacyanochromate Coordination Polymers in Water-in-Oil Microemulsions, *Nano Lett.*, 2002, **2**, 225–229.

137 M. Yamada, M. Arai, M. Kurihara, M. Sakamoto and M. Miyake, Synthesis and Isolation of Cobalt Hexacyanoferrate/Chromate Metal Coordination Nanopolymers Stabilized by Alkylamino Ligand with Metal Elemental Control, *J. Am. Chem. Soc.*, 2004, **126**, 9482–9483.

138 L. Catala, T. Gacoin, J.-P. Boilot, É. Rivière, C. Paulsen, E. Lhotel and T. Mallah, Cyanide-Bridged $Cr^{III}$–$Ni^{II}$ Superparamagnetic Nanoparticles, *Adv. Mater.*, 2003, **15**, 826–829.

139 T. Uemura and S. Kitagawa, Prussian Blue Nanoparticles Protected by Poly(vinylpyrrolidone), *J. Am. Chem. Soc.*, 2003, **125**, 7814–7815.

140 M. Perrier, S. Kenouche, J. Long, K. Thangavel, J. Larionova, C. Goze-Bac, A. Lascialfari, M. Mariani, N. Baril, C. Guérin, B. Donnadieu, A. Trifonov and Y. Guari, Investigation on NMR Relaxivity of Nano-Sized Cyano-Bridged Coordination Polymers, *Inorg. Chem.*, 2013, **52**, 13402–13414.

141 L. Catala, A. Gloter, O. Stephan, G. Rogez and T. Mallah, Superparamagnetic bimetallic cyanide-bridged coordination nanoparticles with $T_B$ = 9 K, *Chem. Commun.*, 2006, 1018–1020, DOI: 10.1039/B516425G.

142 T. Uemura, M. Ohba and S. Kitagawa, Size and Surface Effects of Prussian Blue Nanoparticles Protected by Organic Polymers, *Inorg. Chem.*, 2004, **43**, 7339–7345.

143 E. Chelebaeva, Y. Guari, J. Larionova, A. Trifonov and C. Guérin, Soluble Ligand-Stabilized Cyano-Bridged Coordination Polymer Nanoparticles, *Chem. Mater.*, 2008, **20**, 1367–1375.

144 G. Clavel, J. Larionova, Y. Guari and C. Guérin, Synthesis of Cyano-Bridged Magnetic Nanoparticles Using Room-Temperature Ionic Liquids, *Chem. – Eur. J.*, 2006, **12**, 3798–3804.

145 G. Clavel, Y. Guari, J. Larionova and C. Guerin, Formation of cyano-bridged molecule-based magnetic nanoparticles within hybrid mesoporous silica, *New J. Chem.*, 2005, **29**, 275–279.

146 Y. Guari, J. Larionova, K. Molvinger, B. Folch and C. Guerin, Magnetic water-soluble cyano-bridged metal coordination nano-polymers, *Chem. Commun.*, 2006, 2613–2615, DOI: 10.1039/B602460B.

147 A. Tokarev, P. Agulhon, J. Long, F. Quignard, M. Robitzer, R. A. S. Ferreira, L. D. Carlos, J. Larionova, C. Guérin and Y. Guari, Synthesis and study of Prussian blue type nanoparticles in an alginate matrix, *J. Mater. Chem.*, 2012, **22**, 20232–20242.

148 Y. Xu, Y. Zhang, X. Cai, W. Gao, X. Tang, Y. Chen, J. Chen, L. Chen, Q. Tian and S. Yang, Large-scale synthesis of monodisperse Prussian blue nanoparticles for cancer theranostics via an "in situ modification" strategy, *Int. J. Nanomed.*, 2019, **14**, 271.

149 M. Shokouhimehr, E. S. Soehnlen, J. Hao, M. Griswold, C. Flask, X. Fan, J. P. Basilion, S. Basu and S. D. Huang, Dual purpose Prussian blue nanoparticles for cellular imaging and drug delivery: a new generation of T1-weighted MRI contrast and small molecule delivery agents, *J. Mater. Chem.*, 2010, **20**, 5251–5259.

150 M. Shokouhimehr, E. S. Soehnlen, A. Khitrin, S. Basu and S. D. Huang, Biocompatible Prussian blue nanoparticles: Preparation, stability, cytotoxicity, and potential use as an MRI contrast agent, *Inorg. Chem. Commun.*, 2010, **13**, 58–61.

151 M. Hu, S. Ishihara, K. Ariga, M. Imura and Y. Yamauchi, Kinetically Controlled Crystallization for Synthesis of Monodispersed Coordination Polymer Nanocubes and Their Self-Assembly to Periodic Arrangements, *Chem. – Eur. J.*, 2013, **19**, 1882–1885.

152 S.-Q. Liu, J.-J. Xu and H.-Y. Chen, Electrochemical behavior of nanosized Prussian blue self-assembled on Au electrode surface, *Electrochem. Commun.*, 2002, **4**, 421–425.

153 P. A. Fiorito, V. R. Gonçales, E. A. Ponzio and S. I. C. de Torresi, Synthesis, characterization and immobilization of Prussian blue nanoparticles. A potential tool for biosensing devices, *Chem. Commun.*, 2005, 366–368.

154 D. M. DeLongchamp and P. T. Hammond, High-Contrast Electrochromism and Controllable Dissolution of Assembled Prussian Blue/Polymer Nanocomposites, *Adv. Funct. Mater.*, 2004, **14**, 224–232.

155 Z. Jia and G. Sun, Preparation of prussian blue nanoparticles with single precursor, *Colloids Surf., A*, 2007, **302**, 326–329.

156 D. Brinzei, L. Catala, N. Louvain, G. Rogez, O. Stephan, A. Gloter and T. Mallah, Spontaneous stabilization and isolation of dispersible bimetallic coordination nanoparticles of $Cs_xNi[Cr(CN)_6]_y$, *J. Mater. Chem.*, 2006, **16**, 2593–2599.

157 M. Presle, I. Maurin, F. Maroun, R. Cortès, L. Lu, R. Sayed Hassan, E. Larquet, J.-M. Guigner, E. Rivière, J. P. Wright, J.-P. Boilot and T. Gacoin, Photostrictive/Piezomagnetic

 

Core–Shell Particles Based on Prussian Blue Analogues: Evidence for Confinement Effects?, *J. Phys. Chem. C*, 2014, **118**, 13186–13195.

158 M. F. Dumont, E. S. Knowles, A. Guiet, D. M. Pajerowski, A. Gomez, S. W. Kycia, M. W. Meisel and D. R. Talham, Photoinduced Magnetism in Core/Shell Prussian Blue Analogue Heterostructures of $K_jNi_k[Cr(CN)_6]_l{\cdot}nH_2O$ with $Rb_aCo_b[Fe(CN)_6]_c{\cdot}mH_2O$, *Inorg. Chem.*, 2011, **50**, 4295–4300.

159 Y. Mizuno, M. Okubo, K. Kagesawa, D. Asakura, T. Kudo, H. Zhou, K. Oh-ishi, A. Okazawa and N. Kojima, Precise Electrochemical Control of Ferromagnetism in a Cyanide-Bridged Bimetallic Coordination Polymer, *Inorg. Chem.*, 2012, **51**, 10311–10316.

160 C. H. Li, Y. Nanba, D. Asakura, M. Okubo and D. R. Talham, Li-ion and Na-ion insertion into size-controlled nickel hexacyanoferrate nanoparticles, *RSC Adv.*, 2014, **4**, 24955–24961.

161 G. Paul, Y. Prado, N. Dia, E. Riviere, S. Laurent, M. Roch, L. V. Elst, R. N. Muller, L. Sancey, P. Perriat, O. Tillement, T. Mallah and L. Catala, $Mn^{II}$-containing coordination nanoparticles as highly efficient T1 contrast agents for magnetic resonance imaging, *Chem. Commun.*, 2014, **50**, 6740–6743.

162 G. Felix, W. Nicolazzi, L. Salmon, G. Molnar, M. Perrier, G. Maurin, J. Larionova, J. Long, Y. Guari and A. Bousseksou, Enhanced cooperative interactions at the nanoscale in spin-crossover materials with a first-order phase transition, *Phys. Rev. Lett.*, 2013, **110**, 235701.

163 J. Liang, C. H. Li and D. R. Talham, Growth Mechanisms of Mesoscale Prussian Blue Analogue Particles in Modifier-free Synthesis, *Cryst. Growth Des.*, 2020, **20**, 2713–2720.

164 Y. Prado, L. Lisnard, D. Heurtaux, G. Rogez, A. Gloter, O. Stephan, N. Dia, E. Riviere, L. Catala and T. Mallah, Tailored coordination nanoparticles: assessing the magnetic single-domain critical size, *Chem. Commun.*, 2011, **47**, 1051–1053.

165 Y. Prado, S. Mazerat, E. Rivière, G. Rogez, A. Gloter, O. Stéphan, L. Catala and T. Mallah, Magnetization Reversal in $CsNi^{II}Cr^{III}(CN)_6$ Coordination Nanoparticles: Unravelling Surface Anisotropy and Dipolar Interaction Effects, *Adv. Funct. Mater.*, 2014, **24**, 5402–5411.

166 G. Ngo, G. Félix, J. Long, L. Costa, O. Saavedra V., P.-E. Milhiet, J.-M. Devoisselle, Y. Guari, J. Larionova and J. Chopineau, A simple approach for controlled deposition of Prussian blue analogue nanoparticles on a functionalised plasmonic gold surface, *New J. Chem.*, 2019, **43**, 3660–3664.

167 E. Mamontova, M. Daurat, J. Long, A. Godefroy, F. Salles, Y. Guari, M. Gary-Bobo and J. Larionova, Fashioning Prussian Blue Nanoparticles by Adsorption of Luminophores: Synthesis, Properties, and in Vitro Imaging, *Inorg. Chem.*, 2020, **59**, 4567–4575.

168 Y. Guari, M. Cahu, G. Félix, S. Sene, J. Long, J. Chopineau, J.-M. Devoisselle and J. Larionova, Nanoheterostructures based on nanosized Prussian blue and its Analogues: Design, properties and applications, *Coord. Chem. Rev.*, 2022, **461**, 214497.

169 J. Nai and X. W. Lou, Hollow Structures Based on Prussian Blue and Its Analogs for Electrochemical Energy Storage and Conversion, *Adv. Mater.*, 2019, **31**, 1706825.

170 M. Hu, S. Furukawa, R. Ohtani, H. Sukegawa, Y. Nemoto, J. Reboul, S. Kitagawa and Y. Yamauchi, Synthesis of Prussian Blue Nanoparticles with a Hollow Interior by Controlled Chemical Etching, *Angew. Chem., Int. Ed.*, 2012, **51**, 984–988.

171 G. Liang, J. Xu and X. Wang, Synthesis and Characterization of Organometallic Coordination Polymer Nanoshells of Prussian Blue Using Miniemulsion Periphery Polymerization (MEPP), *J. Am. Chem. Soc.*, 2009, **131**, 5378–5379.

172 R. McHale, Y. Liu, N. Ghasdian, N. S. Hondow, S. Ye, Y. Lu, R. Brydson and X. Wang, Dual lanthanide role in the designed synthesis of hollow metal coordination (Prussian Blue analogue) nanocages with large internal cavity and mesoporous cage, *Nanoscale*, 2011, **3**, 3685–3694.

173 M. Hu, J.-S. Jiang and Y. Zeng, Prussian blue microcrystals prepared by selective etching and their conversion to mesoporous magnetic iron(III) oxides, *Chem. Commun.*, 2010, **46**, 1133–1135.

174 A. Azhar, Y. Li, Z. Cai, M. B. Zakaria, M. K. Masud, M. S. A. Hossain, J. Kim, W. Zhang, J. Na, Y. Yamauchi and M. Hu, Nanoarchitectonics: A New Materials Horizon for Prussian Blue and Its Analogues, *Bull. Chem. Soc. Jpn.*, 2019, **92**, 875–904.

175 M. Hu, A. A. Belik, M. Imura and Y. Yamauchi, Tailored Design of Multiple Nanoarchitectures in Metal-Cyanide Hybrid Coordination Polymers, *J. Am. Chem. Soc.*, 2013, **135**, 384–391.

176 W. Zhang, Y. Zhao, V. Malgras, Q. Ji, D. Jiang, R. Qi, K. Ariga, Y. Yamauchi, J. Liu, J.-S. Jiang and M. Hu, Synthesis of Monocrystalline Nanoframes of Prussian Blue Analogues by Controlled Preferential Etching, *Angew. Chem., Int. Ed.*, 2016, **55**, 8228–8234.

177 L. Han, X.-Y. Yu and X. W. Lou, Formation of Prussian-Blue-Analog Nanocages via a Direct Etching Method and their Conversion into Ni–Co-Mixed Oxide for Enhanced Oxygen Evolution, *Adv. Mater.*, 2016, **28**, 4601–4605.

178 O. N. Risset, E. S. Knowles, S. Ma, M. W. Meisel and D. R. Talham, $Rb_jM_k[Fe(CN)_6]l$ (M = Co, Ni) Prussian Blue Analogue Hollow Nanocubes: a New Example of a Multilevel Pore System, *Chem. Mater.*, 2013, **25**, 42–47.

179 G. Maurin-Pasturel, J. Long, Y. Guari, F. Godiard, M.-G. Willinger, C. Guerin and J. Larionova, Nanosized Heterostructures of Au@Prussian Blue Analogues: Towards Multifunctionality at the Nanoscale, *Angew. Chem., Int. Ed.*, 2014, **53**, 3872–3876.

180 X. Hu, X. Wang, X. Hu, C. Xie and D. Zeng, Structure evolution from Prussian-blue nanocubes to hollow nanocage composites via sodium tungstate etching, *Chem. Commun.*, 2019, **55**, 13386–13389.

181 X. Yin, H. Li, H. Wang, Z. Zhang, R. Yuan, J. Lu, Q. Song, J.-G. Wang, L. Zhang and Q. Fu, Self-Templating Synthesis of Cobalt Hexacyanoferrate Hollow Structures with Superior Performance for Na-Ion Hybrid Supercapacitors, *ACS Appl. Mater. Interfaces*, 2018, **10**, 29496–29504.

182 A. Gotoh, H. Uchida, M. Ishizaki, T. Satoh, S. Kaga, S. Okamoto, M. Ohta, M. Sakamoto, T. Kawamoto, H. Tanaka, M. Tokumoto, S. Hara, H. Shiozaki, M. Yamada, M. Miyake and M. Kurihara, Simple synthesis of three primary colour nanoparticle inks of Prussian blue and its analogues, *Nanotechnology*, 2007, **18**, 345609.

183 M. Ishizaki, K. Kanaizuka, M. Abe, Y. Hoshi, M. Sakamoto, T. Kawamoto, H. Tanaka and M. Kurihara, Preparation of electrochromic Prussian blue nanoparticles dispersible into various solvents for realisation of printed electronics, *Green Chem.*, 2012, **14**, 1537–1544.

184 W.-P. Li, C.-H. Su, L.-C. Tsao, C.-T. Chang, Y.-P. Hsu and C.-S. Yeh, Controllable CO Release Following Near-Infrared Light-Induced Cleavage of Iron Carbonyl Derivatized Prussian Blue Nanoparticles for CO-Assisted Synergistic Treatment, *ACS Nano*, 2016, **10**, 11027–11036.

185 G. Maurin-Pasturel, E. Rascol, M. Busson, S. Sevestre, J. Lai-Kee-Him, P. Bron, J. Long, J. Chopineau, J.-M. Devoisselle, Y. Guari and J. Larionova, $^{201}$Tl-labeled Prussian blue and Au@Prussian blue nanoprobes for SPEC-CT imaging: influence of the size, shape and coating on the biodistribution, *Inorg. Chem. Front.*, 2017, **4**, 1737–1741.

186 T. Kim, J. E. Lemaster, F. Chen, J. Li and J. V. Jokerst, Photoacoustic Imaging of Human Mesenchymal Stem Cells Labeled with Prussian Blue-Poly(l-lysine) Nanocomplexes, *ACS Nano*, 2017, **11**, 9022–9032.

187 M. Shokouhimehr, E. S. Soehnlen, A. Khitrin, S. Basu and S. D. Huang, Biocompatible Prussian blue nanoparticles: Preparation, stability, cytotoxicity, and potential use as an MRI contrast agent, *Inorg. Chem. Commun.*, 2010, **13**, 58–61.

188 S.-J. Wang, C.-S. Chen and L.-C. Chen, Prussian blue nanoparticles as nanocargoes for delivering DNA drugs to cancer cells, *Sci. Technol. Adv. Mater.*, 2013, **14**, 044405.

189 L. Cheng, H. Gong, W. Zhu, J. Liu, X. Wang, G. Liu and Z. Liu, PEGylated Prussian blue nanocubes as a theranostic agent for simultaneous cancer imaging and photothermal therapy, *Biomaterials*, 2014, **35**, 9844–9852.

190 W. Zhu, K. Liu, X. Sun, X. Wang, Y. Li, L. Cheng and Z. Liu, $Mn^{2+}$-Doped Prussian Blue Nanocubes for Bimodal Imaging and Photothermal Therapy with Enhanced Performance, *ACS Appl. Mater. Interfaces*, 2015, **7**, 11575–11582.

191 H. Chen, Y. Ma, X. Wang, X. Wu and Z. Zha, Facile synthesis of Prussian blue nanoparticles as pH-responsive drug carriers for combined photothermal-chemo treatment of cancer, *RSC Adv.*, 2017, **7**, 248–255.

192 R. A. Burga, S. Patel, C. M. Bollard, C. R. Y. Cruz and R. Fernandes, Conjugating Prussian blue nanoparticles onto antigen-specific T cells as a combined nanoimmunotherapy, *Nanomedicine*, 2016, **11**, 1759–1767.

193 V. S. Perera, G. Chen, Q. Cai and S. D. Huang, Nanoparticles of gadolinium-incorporated Prussian blue with PEG coating as an effective oral MRI contrast agent for gastrointestinal tract imaging, *Analyst*, 2016, **141**, 2016–2022.

194 L. Jing, S. Shao, Y. Wang, Y. Yang, X. Yue and Z. Dai, Hyaluronic Acid Modified Hollow Prussian Blue Nanoparticles Loading 10-hydroxycamptothecin for Targeting Thermochemotherapy of Cancer, *Theranostics*, 2016, **6**, 40–53.

195 J. Peng, Q. Yang, W. Li, L. Tan, Y. Xiao, L. Chen, Y. Hao and Z. Qian, Erythrocyte-Membrane-Coated Prussian Blue/Manganese Dioxide Nanoparticles as $H_2O_2$-Responsive Oxygen Generators To Enhance Cancer Chemotherapy/Photothermal Therapy, *ACS Appl. Mater. Interfaces*, 2017, **9**, 44410–44422.

196 Z. Li, Y. Hu, T. Jiang, K. A. Howard, Y. Li, X. Fan, Y. Sun, F. Besenbacher and M. Yu, Human-Serum-Albumin-Coated Prussian Blue Nanoparticles as pH-/Thermotriggered Drug-Delivery Vehicles for Cancer Thermochemotherapy, *Part. Part. Syst. Charact.*, 2016, **33**, 53–62.

197 X. Lin, Y. Cao, J. Li, D. Zheng, S. Lan, Y. Xue, F. Yu, M. Wu and X. Zhu, Folic acid-modified Prussian blue/polydopamine nanoparticles as an MRI agent for use in targeted chemo/photothermal therapy, *Biomater. Sci.*, 2019, **7**, 2996–3006.

198 Y. Wang, X. Pang, J. Wang, Y. Cheng, Y. Song, Q. Sun, Q. You, F. Tan, J. Li and N. Li, Magnetically-targeted and near infrared fluorescence/magnetic resonance/photoacoustic imaging-guided combinational anti-tumor phototherapy based on polydopamine-capped magnetic Prussian blue nanoparticles, *J. Mater. Chem. B*, 2018, **6**, 2460–2473.

199 P. Xue, L. Sun, Q. Li, L. Zhang, Z. Xu, C. M. Li and Y. Kang, PEGylated magnetic Prussian blue nanoparticles asa multifunctional therapeutic agent for combined targeted photothermal ablation and pH-triggered chemotherapy of tumour cells, *J. Colloid Interface Sci.*, 2018, **509**, 384–394.

200 Z. Gao, Y. Li, C. Zhang, S. Zhang, Y. Jia and Y. Dong, An enzyme-free immunosensor for sensitive determination of procalcitonin using NiFe PBA nanocubes@TB as the sensing matrix, *Anal. Chim. Acta*, 2020, **1097**, 169–175.

201 Y. Li, R. Guo, C. Deng, D. Li and H. Wu, A Prussian Blue Nanoparticles-based Fluorescent Nanoprobe for Monitoring MicroRNA-92a and MicroRNA-21, *Anal. Sci.*, 2022, **38**, 497–504.

202 M. F. Dumont, H. A. Hoffman, P. R. S. Yoon, L. S. Conklin, S. R. Saha, J. Paglione, R. W. Sze and R. Fernandes, Biofunctionalized Gadolinium-Containing Prussian Blue Nanoparticles as Multimodal Molecular Imaging Agents, *Bioconjugate Chem.*, 2014, **25**, 129–137.

203 M. F. Dumont, S. Yadavilli, R. W. Sze, J. Nazarian and R. Fernandes, Manganese-containing Prussian blue nanoparticles for imaging of pediatric brain tumors, *Int. J. Nanomed.*, 2014, **9**, 2581–2595.

204 P. Nie, J. Yuan, J. Wang, Z. Le, G. Xu, L. Hao, G. Pang, Y. Wu, H. Dou, X. Yan and X. Zhang, Prussian Blue Analogue with Fast Kinetics Through Electronic Coupling for Sodium Ion Batteries, *ACS Appl. Mater. Interfaces*, 2017, **9**, 20306–20312.

205 Y. Yang, L. Jing, X. Li, L. Lin, X. Yue and Z. Dai, Hyaluronic Acid Conjugated Magnetic Prussian Blue@Quantum Dot Nanoparticles for Cancer Theranostics, *Theranostics*, 2017, **7**, 466–481.

206 X. Li, X. Yue, J. Wang, X. Liang, L. Jing, L. Lin, Y. Yang, S. Feng, Y. Qian and Z. Dai, Prussian blue nanoparticle-loaded microbubbles for photothermally enhanced gene delivery through ultrasound-targeted microbubble destruction, *Sci. Bull.*, 2016, **61**, 148–156.

207 Z. Li, Y. Zeng, D. Zhang, M. Wu, L. Wu, A. Huang, H. Yang, X. Liu and J. Liu, Glypican-3 antibody functionalized Prussian blue nanoparticles for targeted MR imaging and photothermal therapy of hepatocellular carcinoma, *J. Mater. Chem. B*, 2014, **2**, 3686–3696.

208 O. Akbal, G. Bolat, Y. T. Yaman and S. Abaci, Folic acid conjugated Prussian blue nanoparticles: Synthesis, physicochemical characterization and targeted cancer cell sensing, *Colloids Surf., B*, 2020, **187**, 110655.

209 L. Forgách, N. Hegedűs, I. Horváth, B. Kiss, N. Kovács, Z. Varga, G. Jakab, T. Kovács, P. Padmanabhan, K. Szigeti and D. Máthé, Fluorescent, Prussian Blue-Based Biocompatible Nanoparticle System for Multimodal Imaging Contrast, *Nanomaterials*, 2020, **10**, 1732.

210 A. Sahu, J. H. Lee, H. G. Lee, Y. Y. Jeong and G. Tae, Prussian blue/serum albumin/indocyanine green as a multifunctional nanotheranostic agent for bimodal imaging guided laser mediated combinatorial phototherapy, *J. Controlled Release*, 2016, **236**, 90–99.

211 H.-Y. Lian, M. Hu, C.-H. Liu, Y. Yamauchi and K. C. W. Wu, Highly biocompatible, hollow coordination polymer nanoparticles as cisplatin carriers for efficient intracellular drug delivery, *Chem. Commun.*, 2012, **48**, 5151–5153.

212 X. Cai, X. Jia, W. Gao, K. Zhang, M. Ma, S. Wang, Y. Zheng, J. Shi and H. Chen, A Versatile Nanotheranostic Agent for Efficient Dual-Mode Imaging Guided Synergistic Chemo-Thermal Tumor Therapy, *Adv. Funct. Mater.*, 2015, **25**, 2520–2529.

213 M. Wu, Q. Wang, X. Liu and J. Liu, Highly efficient loading of doxorubicin in Prussian Blue nanocages for combined photothermal/chemotherapy against hepatocellular carcinoma, *RSC Adv.*, 2015, **5**, 30970–30980.

214 W. Chen, K. Zeng, H. Liu, J. Ouyang, L. Wang, Y. Liu, H. Wang, L. Deng and Y.-N. Liu, Cell Membrane Camouflaged Hollow Prussian Blue Nanoparticles for Synergistic Photothermal-/Chemotherapy of Cancer, *Adv. Funct. Mater.*, 2017, **27**, 1605795.

215 Y. Ma, H. Chen, B. Hao, J. Zhou, G. He, Z. Miao, Y. Xu, L. Gao, W. Zhou and Z. Zha, A chloroquine-loaded Prussian blue platform with controllable autophagy inhibition for enhanced photothermal therapy, *J. Mater. Chem. B*, 2018, **6**, 5854–5859.

216 H. Chen, Y. Ma, X. Wang and Z. Zha, Multifunctional phase-change hollow mesoporous Prussian blue nanoparticles as a NIR light responsive drug co-delivery system to overcome cancer therapeutic resistance, *J. Mater. Chem. B*, 2017, **5**, 7051–7058.

217 J. Li, F. Zhang, Z. Hu, W. Song, G. Li, G. Liang, J. Zhou, K. Li, Y. Cao, Z. Luo and K. Cai, Drug "Pent-Up" in Hollow Magnetic Prussian Blue Nanoparticles for NIR-Induced Chemo-Photothermal Tumor Therapy with Trimodal Imaging, *Adv. Healthcare Mater.*, 2017, **6**, 1700005.

218 M. Perrier, M. Busson, G. Massasso, J. Long, V. Boudousq, J. P. Pouget, S. Peyrottes, C. Perigaud, C. Porredon-Guarch, J. de Lapuente, M. Borras, J. Larionova and Y. Guari, $^{201}Tl^{+}$-labelled Prussian blue nanoparticles as contrast agents for SPECT scintigraphy, *Nanoscale*, 2014, **6**, 13425–13429.

219 E. Mamontova, J. Long, R. A. S. Ferreira, A. M. P. Botas, F. Salles, Y. Guari, L. D. Carlos and J. Larionova, Making Prussian blue analogues nanoparticles luminescent: effect of the luminophore confinement over the properties, *Nanoscale*, 2019, **11**, 7097–7101.

220 R. Yang, M. Hou, Y. Gao, L. Zhang, Z. Xu, Y. Kang and P. Xue, Indocyanine green-modified hollow mesoporous Prussian blue nanoparticles loading doxorubicin for fluorescence-guided tri-modal combination therapy of cancer, *Nanoscale*, 2019, **11**, 5717–5731.

221 L. M. A. Ali, E. Mathlouthi, M. Cahu, S. Sene, M. Daurat, J. Long, Y. Guari, F. Salles, J. Chopineau, J.-M. Devoisselle, J. Larionova and M. Gary-Bobo, Synergic effect of doxorubicin release and two-photon irradiation of $Mn^{2+}$-doped Prussian blue nanoparticles on cancer therapy, *RSC Adv.*, 2020, **10**, 2646–2649.

222 W. P. Lustig, S. Mukherjee, N. D. Rudd, A. V. Desai, J. Li and S. K. Ghosh, Metal–organic frameworks: functional luminescent and photonic materials for sensing applications, *Chem. Soc. Rev.*, 2017, **46**, 3242–3285.

223 E. Mamontova, J. Long, R. Ferreira, A. M. P. Botas, F. Salles, Y. Guari, L. A. D. Carlos and J. Larionova, Making Prussian blue analogues nanoparticles luminescent: effect of the luminophore confinement over the properties, *Nanoscale*, 2019, **11**, 7097–7101.

224 A. Takahashi, H. Tanaka and T. Kawamoto, *Prussian Blue-Type Nanoparticles and Nanocomposites: Synthesis, Devices, and Applications*, 2019, p. 217.

225 X. Cai, W. Gao, L. Zhang, M. Ma, T. Liu, W. Du, Y. Zheng, H. Chen and J. Shi, Enabling Prussian Blue with Tunable Localized Surface Plasmon Resonances: Simultaneously Enhanced Dual-Mode Imaging and Tumor Photothermal Therapy, *ACS Nano*, 2016, **10**, 11115–11126.

226 M. Perrier, A. Gallud, A. Ayadi, S. Kennouche, C. Porredon, M. Gary-Bobo, J. Larionova, C. Goze-Bac,

M. Zanca, M. Garcia, I. Basile, J. Long, J. de Lapuente, M. Borras and Y. Guari, Investigation of cyano-bridged coordination nanoparticles $Gd^{3+}/[Fe(CN)_6]^{3-}$/d-mannitol as $T_1$-weighted MRI contrast agents, *Nanoscale*, 2015, **7**, 11899–11903.

227 E. Chelebaeva, J. Larionova, Y. Guari, R. A. S. Ferreira, L. D. Carlos, A. A. Trifonov, T. Kalaivani, A. Lascialfari, C. Guerin, K. Molvinger, L. Datas, M. Maynadier, M. Gary-Bobo and M. Garcia, Nanoscale coordination polymers exhibiting luminescence properties and NMR relaxivity, *Nanoscale*, 2011, **3**, 1200–1210.

228 Y. Guari, J. Larionova, M. Corti, A. Lascialfari, M. Marinone, G. Poletti, K. Molvinger and C. Guerin, Cyano-bridged coordination polymer nanoparticles with high nuclear relaxivity: toward new contrast agents for MRI, *Dalton Trans.*, 2008, 3658–3660.

229 Y. Li, C. H. Li and D. R. Talham, One-step synthesis of gradient gadolinium ironhexacyanoferrate nanoparticles: a new particle design easily combining MRI contrast and photothermal therapy, *Nanoscale*, 2015, **7**, 5209–5216.

230 Z. Qin, B. Chen, X. Huang, Y. Mao, Y. Li, F. Yang and N. Gu, Magnetic internal heating-induced high performance Prussian blue nanoparticle preparation and excellent catalytic activity, *Dalton Trans.*, 2019, **48**, 17169–17173.

231 L. Jing, X. Liang, Z. Deng, S. Feng, X. Li, M. Huang, C. Li and Z. Dai, Prussian blue coated gold nanoparticles for simultaneous photoacoustic/CT bimodal imaging and photothermal ablation of cancer, *Biomaterials*, 2014, **35**, 5814–5821.

232 X. Liang, Z. Deng, L. Jing, X. Li, Z. Dai, C. Li and M. Huang, Prussian blue nanoparticles operate as a contrast agent for enhanced photoacoustic imaging, *Chem. Commun.*, 2013, **49**, 11029–11031.

233 M. S. Kandanapitiye, F. J. Wang, B. Valley, C. Gunathilake, M. Jaroniec and S. D. Huang, Selective Ion Exchange Governed by the Irving–Williams Series in $K_2Zn_3[Fe(CN)_6]_2$ Nanoparticles: Toward a Designer Prodrug for Wilson's Disease, *Inorg. Chem.*, 2015, **54**, 1212–1214.

234 C. Lavaud, M. Kajdan, E. Compte, J.-C. Maurel, J. Laikeehim, P. Bron, E. Oliviero, J. Long, J. Larionova and Y. Guari, In situ synthesis of Prussian blue nanoparticles within a biocompatible reverse micellar system for in vivo $Cs^+$ uptake, *New J. Chem.*, 2017, **41**, 2887–2890.

235 S. Mukherjee, B. R. Rao, B. Sreedhar, P. Paik and C. R. Patra, Copper Prussian blue analogue: investigation into multifunctional activities for biomedical applications, *Chem. Commun.*, 2015, **51**, 7325–7328.

236 W. Shao-Jen, C. Chun-Sheng and C. Lin-Chi, Prussian blue nanoparticles as nanocargoes for delivering DNA drugs to cancer cells, *Sci. Technol. Adv. Mater.*, 2013, **14**, 044405.

237 A. M. Alkilany, L. B. Thompson, S. P. Boulos, P. N. Sisco and C. J. Murphy, Gold nanorods: Their potential for photothermal therapeutics and drug delivery, tempered by the complexity of their biological interactions, *Adv. Drug Delivery Rev.*, 2012, **64**, 190–199.

238 V. Shanmugam, S. Selvakumar and C.-S. Yeh, Near-infrared light-responsive nanomaterials in cancer therapeutics, *Chem. Soc. Rev.*, 2014, **43**, 6254–6287.

239 L. M. A. Ali, E. Mathlouthi, M. Kajdan, M. Daurat, J. Long, R. Sidi-Boulenouar, M. Cardoso, C. Goze-Bac, N. Amdouni, Y. Guari, J. Larionova and M. Gary-Bobo, Multifunctional manganese-doped Prussian blue nanoparticles for two-photon Photothermal Therapy and Magnetic Resonance Imaging, *Photodiagn. Photodyn. Ther.*, 2018, **22**, 65–69.

240 L. Zou, H. Wang, B. He, L. Zeng, T. Tan, H. Cao, X. He, Z. Zhang, S. Guo and Y. Li, Current Approaches of Photothermal Therapy in Treating Cancer Metastasis with Nanotherapeutics, *Theranostics*, 2016, **6**, 762–772.

241 B. Liu, W. Wang, J. Fan, Y. Long, F. Xiao, M. Daniyal, C. Tong, Q. Xie, Y. Jian, B. Li, X. Ma and W. Wang, RBC membrane camouflaged prussian blue nanoparticles for gamabutolin loading and combined chemo/photothermal therapy of breast cancer, *Biomaterials*, 2019, **217**, 119301.

242 X. Chen, G. Wu, J. Tang, L. Zhou and S. Wei, Ytterbium – Doped Prussian blue: Fabrication, photothermal performance and antibacterial activity, *Inorg. Chem. Commun.*, 2020, **114**, 107821.

243 S.-J. Wang, C.-S. Chen and L.-C. Chen, Prussian blue nanoparticles as nanocargoes for delivering DNA drugs to cancer cells, *Sci. Technol. Adv. Mater.*, 2013, **14**, 044405.

244 S. Rojas, I. Colinet, D. Cunha, T. Hidalgo, F. Salles, C. Serre, N. Guillou and P. Horcajada, Toward Understanding Drug Incorporation and Delivery from Biocompatible Metal–Organic Frameworks in View of Cutaneous Administration, *ACS Omega*, 2018, **3**, 2994–3003.

245 P. H. Ho, F. Salles, F. Di Renzo and P. Trens, One-pot synthesis of 5-FU@ZIF-8 and ibuprofen@ZIF-8 nanoparticles, *Inorg. Chim. Acta*, 2020, **500**, 119229.

246 A. Botet-Carreras, C. Tamames-Tabar, F. Salles, S. Rojas, E. Imbuluzqueta, H. Lana, M. J. Blanco-Prieto and P. Horcajada, Improving the genistein oral bioavailability via its formulation into the metal–organic framework MIL-100(Fe), *J. Mater. Chem. B*, 2021, **9**, 2233–2239.

247 M. C. Bernini, D. Fairen-Jimenez, M. Pasinetti, A. J. Ramirez-Pastor and R. Q. Snurr, Screening of biocompatible metal–organic frameworks as potential drug carriers using Monte Carlo simulations, *J. Mater. Chem. B*, 2014, **2**, 766–774.

248 C. D. S. Brites, P. P. Lima, N. J. O. Silva, A. Millán, V. S. Amaral, F. Palacio and L. D. Carlos, Thermometry at the nanoscale, *Nanoscale*, 2012, **4**, 4799–4829.

249 D. Jaque and F. Vetrone, Luminescence nanothermometry, *Nanoscale*, 2012, **4**, 4301–4326.

250 C. D. S. Brites, S. Balabhadra and L. D. Carlos, Lanthanide-Based Thermometers: At the Cutting-Edge of Luminescence Thermometry, *Adv. Opt. Mater.*, 2019, **7**, 1801239.

251 C. A. Kerr and R. de la Rica, Photoluminescent nanosensors for intracellular detection, *Anal. Methods*, 2015, **7**, 7067–7075.

 

252 Y. Guo and W. Zhao, Nanomaterials for luminescent detection of water and humidity, *Analyst*, 2019, **144**, 388–395.

253 T. T. Basiev, I. T. Basieva and M. E. Doroshenko, Luminescent nanophotonics and advanced solid state lasers, *J. Lumin.*, 2013, **133**, 233–243.

254 J. Probst, S. Dembski, M. Milde and S. Rupp, Luminescent nanoparticles and their use for in vitro and in vivo diagnostics, *Expert Rev. Mol. Diagn.*, 2012, **12**, 49–64.

255 F. Leblond, S. C. Davis, P. A. Valdés and B. W. Pogue, Pre-clinical whole-body fluorescence imaging: Review of instruments, methods and applications, *J. Photochem. Photobiol., B*, 2010, **98**, 77–94.

256 M. B. Robin and P. Day, in *Advances in Inorganic Chemistry and Radiochemistry*, ed. H. J. Emeléus and A. G. Sharpe, Academic Press, 1968, vol. 10, pp. 247–422.

257 J. N. Behera, D. M. D'Alessandro, N. Soheilnia and J. R. Long, Synthesis and Characterization of Ruthenium and Iron–Ruthenium Prussian Blue Analogues, *Chem. Mater.*, 2009, **21**, 1922–1926.

258 S. Wu, X. Shen, Z. Xu, J. Wu and C. Gao, Microrods based on nanocubes of Prussian blue, *Appl. Surf. Sci.*, 2009, **255**, 9182–9185.

259 S. Ye, Y. Liu, S. Chen, S. Liang, R. McHale, N. Ghasdian, Y. Lu and X. Wang, Photoluminescent properties of Prussian Blue (PB) nanoshells and polypyrrole (PPy)/PB core/shell nanoparticles prepared via miniemulsion (periphery) polymerization, *Chem. Commun.*, 2011, **47**, 6831–6833.

260 M. Verdaguer and G. S. Girolami, *Magnetism: Molecules to Materials V*, Wiley-VCH Verlag GmbH & Co. KGaA, 2005, pp. 283–346. DOI: **10.1002/3527604383.ch9**.

261 F. Pointillart, O. Cador, B. Le Guennic and L. Ouahab, Uncommon lanthanide ions in purely 4f Single Molecule Magnets, *Coord. Chem. Rev.*, 2017, **346**, 150–175.

262 J. Long, Y. Guari, R. A. S. Ferreira, L. D. Carlos and J. Larionova, Recent advances in luminescent lanthanide based Single-Molecule Magnets, *Coord. Chem. Rev.*, 2018, **363**, 57–70.

263 K. Kumar, S. Chorazy, K. Nakabayashi, H. Sato, B. Sieklucka and S.-i. Ohkoshi, TbCo and $Tb_{0.5}Dy_{0.5}Co$ layered cyanido-bridged frameworks for construction of colorimetric and ratiometric luminescent thermometers, *J. Mater. Chem. C*, 2018, **6**, 8372–8384.

264 J. Long, Luminescent Schiff-Base Lanthanide Single-Molecule Magnets: The Association Between Optical and Magnetic Properties, *Front. Chem.*, 2019, **7**, 63.

265 J.-H. Jia, Q.-W. Li, Y.-C. Chen, J.-L. Liu and M.-L. Tong, Luminescent single-molecule magnets based on lanthanides: Design strategies, recent advances and magneto-luminescent studies, *Coord. Chem. Rev.*, 2019, **378**, 365–381.

266 R. Marin, G. Brunet and M. Murugesu, Shining New Light on Multifunctional Lanthanide Single-Molecule Magnets, *Angew. Chem., Int. Ed.*, 2021, **60**, 1728–1746.

267 J. Cattermull, S. Wheeler, K. Hurlbutt, M. Pasta and A. L. Goodwin, Filling vacancies in a Prussian blue analogue using mechanochemical post-synthetic modification, *Chem. Commun.*, 2020, **56**, 7873–7876.

268 A. M. Fracaroli, P. Siman, D. A. Nagib, M. Suzuki, H. Furukawa, F. D. Toste and O. M. Yaghi, Seven Post-synthetic Covalent Reactions in Tandem Leading to Enzyme-like Complexity within Metal–Organic Framework Crystals, *J. Am. Chem. Soc.*, 2016, **138**, 8352–8355.